# Simulation and practical implementation of a BMS for a Li-Ion Battery

by

Germán Gómez Armayor

Submitted to the Department of Electrical Engineering, Electronics, Computers and Systems
in partial fulfillment of the requirements for the degree of
Master of Science in Electrical Energy Conversion and Power Systems
at the
UNIVERSIDAD DE OVIEDO
July 2017



Author .....

Certified by .....
David Díaz Reigosa
Associate Professor
Thesis Supervisor

Certified by .....
Daniel Fernández Alonso
Phd
Thesis Supervisor

# Simulation and practical implementation of a BMS for a Li-Ion Battery

by

Germán Gómez Armayor

Submitted to the Department of Electrical Engineering, Electronics, Computers and Systems
on July 22, 2017, in partial fulfillment of the
requirements for the degree of
Master of Science in Electrical Energy Conversion and Power Systems

## Abstract

Batteries are widely used as an electrical energy storage systems. Electric vehicles and distributed generation development are highly related to battery developments. Since a battery are an active element and non-linear system, the internal impedance variation is a key element from the electrical point of view. This deviation could produce resonance with other system elements or affect regulator dynamics. The aim of this thesis is to study the internal impedance of LiFePO4 electrochemical cells for a different operation points and at different frequencies. On top of that, this thesis also deals with cell balancing circuits. Battery packs are made by a group of cells. Imbalance of these cells are very usual, producing extra energy in some cells and deficit energy in others, making the whole battery pack inefficient and reducing its life. An active cell balancing circuit have been designed and tested in the lab.

Thesis Supervisor: David Díaz Reigosa
Title: Associate Professor

Thesis Supervisor: Daniel Fernández Alonso
Title: Phd

# Acknowledgments

Me gustaría empezar agradeciendo a todos los coordinadores del master EECPS por su buen hacer y su gran trabajo. A Fernando Briz del Blanco y por supuesto a mi tutor David Díaz Reigosa por darme la oportunidad de formar parte del grupo de investigación AECP, y por toda su aportación y conocimiento. A María Martínez Gómez mi amiga y compañera de fatigas de estudio por sacarme una sonrisa en los momentos de más estrés y a Cristina González Moral por ser una persona genial y por participar activamente en el desarrollo de esta tesis. Doy las gracias especialmente a Daniel Fernández Alonso por su inestimable ayuda siempre que lo necesité tanto en lo profesional como en lo personal, por su infinita paciencia y por todo lo que aprendí de él. Dicen que ningún hombre es pobre salvo el que carece de sabiduría o conocimiento, por lo que él es muy rico y yo hoy un poco menos pobre, gracias. Por supuesto agradezco a toda mi familia por su apoyo y en especial a mi mujer Sara por ser el pilar en el que me apoyo todos los días.

# Contents

# List of Figures

# List of Tables

# Glossary

### Acronyms

| | |
|---|---|
| **BMS** | Battery management System |
| **EES** | Electrical Energy Storage |
| **EV** | Electric Vehicle |
| **NiMH** | Niquel metal Hydroxide |
| **NiCd** | Niquel Cadmium |
| **LiFePo4** | Lithium Ferro Phosphate |
| **IR** | Internal Resistance |
| **EIS** | Electrical Impedance Spectroscopy |
| **SOC** | State of Charge |
| **SOH** | State of Health |
| **B2B** | Buck to Buck |
| **OCV** | Open Circuit Voltage |
| **DAB** | Dual Active Bridge |
| **SC** | Switched Capacitor |
| **PI** | Proportional Integrator |
| **PWM** | Pulse Width Modulation |
| **ADC** | Analog to Digital Converter |
| **FFT** | Fast Fourier Transform |

# Chapter 1

# Introduction

The rapid developed in intelligent networks, EV, microgrids and the capacity of using different energy sources imply that many systems work in an autonomous way and isolated from the grid. This is satisfied with energy storage systems being a battery one of the most popular.

The battery is a quite old system to storage energy when Alessandro Volta discover the first voltaic cell in 1800. This technology has been rapidly developed until nowadays, using different chemical process to produce energy. Lithium ion batteries (LIB) are widely used in many recent application such as EV and EES due to the benefits compared to other battery types. LIBs are characterized by a high specific energy ($200Wh/kg$), high energy density ($600Wh/L$), good efficiency($\geq$90%), long life cycle($\geq$1000) and relative low cost [3]. Inside this family there are different nomenclature, using always the lithium as an electrolyte but changing the cathode material. In this project the battery under study are Lithium phosphate (LiFePO4).

Batteries used in EES or EV, required large power and energy capacity. The LiFePO4 nominal voltage cell and capacity is in the range of $2.4V - 3.65V$, respectively so the whole battery pack is formed by cells placed in series or parallel according to the configuration and power desired. This type of architecture implies the use of a battery management system (BMS) which is in charge of measuring voltage, current and temperature. A battery pack is made by a group of cells and imbalance of these cells are very usual. Voltage cell and current provides information about that

imbalance, and then it is used to control the operational conditions of the battery pack to prolong its life and guarantee its safety [4].

## 1.1 Objectives and thesis structure

This thesis is part of the project "Advanced plug-and-play off-grid energy generation system and AOO Renewable (OG+)" financed by the ministry of economy and competitiveness. Institutions participating are: Elinsa, Norvento enerxía and University of Oviedo.

The Project will consist on the simulation and practical implementation of a BMS for a Li-Ion battery as well as the study of dynamic performance of the battery and its difference comparing to static models. Fig.1-1 shows the general scheme. It consists in a large scale storage energy system based on batteries. The whole battery is built by 15 modules and each module is formed by 15x15 cells, it means 255 cells in total per module. According to specifications of the project the operation can be done either connecting 7 modules through a buck boost DC-DC converter and LCL filter, using the power converter to boost the voltage or connecting directly the entire pack to the DC bus. A LCL filter is used because it shows better attenuation and reduced size compare to a simple L filter, however as a capacitor is included resonances could appear. The DC link is pre-charged through a resistance and its voltage is measured and controlled all the time, this DC voltage is then passed through an inverter to the grid. As power converters are both bidirectional the energy can flow in both direction it means that the battery is able to either deliver or absorb energy from the grid.

The Buck to buck (B2B) converter is controlled by pulse sine width modulation (PWM) being the switching frequency ($F_{sw}$ = 15kHz), the power converter must handle $100Kw$ of power. To a properly operation of a system and to control the energy flow, variables such as power, voltage and current must be regulated. This is done by control techniques and plant models must be established. Passive elements like inductances, capacitances or resistances are easily known, however a battery is an active element whose internal impedance changes with the operation point. Before

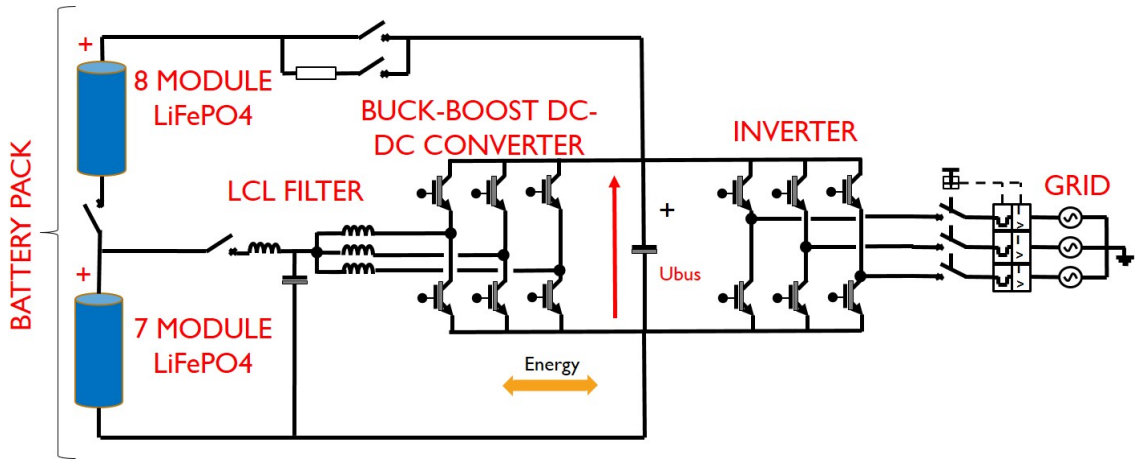


Figure 1-1: Energy electric storage system and supported grid.

the BMS implementation, the first part of this thesis is focused on how the behaviour of a cell moves from its static model at difference rates of charging / discharging currents. This is important for both, to have the knowledge of the plant model to tune regulators and to know the impedance of the battery in order to avoid resonance with other elements of the system.

As it was mentioned before, the main target of this master thesis is to get a static model of the cells provided by the manufacturer (CEGASA), compare this model with a dynamic model in order to get a map of impedance variation for converter designers and finally a BMS implementation at the cell level. The objective will be addressed by the following parts.

- **State of the art:** In this part a review of BMS and battery models have been done. For this purpose, distinct platforms have been consulted such as, google scholar or the association of institution of electric and electronic engineering(IEEE).

- **Static and dynamic model:** According to the bibliography consulted, the first step was to developed a model for a our chemical cell (LiFePO4). All of the models found are referred to static behaviour of a battery so the second thing was to compare this information to dynamic performances. To achieve it, a small-scale of the converter has been built in the lab. Experimental results

are presented.

- **BMS implementation:** Moving on to the next section, a cell equalization method is implemented in the lab. Results are displayed and compared.

# Chapter 2

# State of the art

The first part of this section deals with a brief description of battery types. The second part is related to battery models and finally, the battery management system (BMS) is presented, making a little review about the technology available.

## 2.1 Batteries

As stated previously, electric energy storage systems (EESS) are widely used in EV and systems working isolated to the grid, being batteries one of the most popular. Batteries can be divided into two major categories primary and secondary batteries. Primary batteries are non-rechargeable, whereas secondary batteries are rechargeable. Each battery system is characterized by its chemistry. The present thesis is focused on secondary batteries. Example of secondary batteries are lead-acid (SLA), NiCd, NiMH, Li-ion, Li-ion-polymer, Li-metal, zinc-alkaline-MnO2 [5].

The NiCd battery is commonly known as relatively cheap and robust, with a short period of charge and high power deliver. However these kind of batteries suffers from memory effect and theri energy density and specific energy are relatively low [6] [5].

NiMH present some advantage compare to Niquel Cadmium batteries. it has higher energy density, low internal impedance and it has no memory effect. Nevertheless, they cannot charge as fast as NiCd batteries and overcharging could deteriorate the battery. Li-ion batteries have a relatively high specific energy and power density,

which results in batteries that are smaller than Ni based batteries at the same capacity. On top of that, they can be deep cycled , it means that, the cell maintains a constant voltage for over 80 of its discharge curve, it can be discharged at 40C and its cycle of life is very large. The Positive electrode of a Li-ion battery consists of one of a number of lithium metal oxides, which can store lithium ions. The oxides encountered most frequently in commerciallu available batteries are lithium cobalt oxide (LiCoO2), lithium nickel oxide (LiNiO2), lithium manganese oxide (LiMn2O4) or lithium iron phosphate (LiFePO4). The negative electrode in Li-ion batteries is a carbon electrode [3]. LiFePO4 based batteries are considered to be one of the most valuable lithium-ion batteries in the market, because of their high energy density, lack of memory effect, lower self-discharge, long lifetime, large cycle life number, inherently safe cathode structure under critical conditions, and non-polluting characteristics [7][6]. Overviwe of the main characteristics of a secondary battery systems

Table 2.1: Overview of the main characteristics of a secondary battery systems

| Battery | **NiCd** | **NiMH** | **Li-ion** | **Li-poly** | **Lead Acid** |
|---|---|---|---|---|---|
| **Energy density (Wh/l)** | 90-150 | 160-310 | 200-300 | 200-250 | 90-160 |
| **Specific Energy (Wh/kg)** | 30-60 | 50-90 | 90-115 | 100-115 | 30-50 |
| **Fast charge time** | 1h | 2-4h | 2-4h | 2-4h | 8-15h |
| **Cycle life** | 300-700 | 300-600 | 500-1000 | 200 | 200-300 |
| **Cost per cycle(dollar)** | 0.04 | 0.12 | 0.14 | 0.29 | 0.10 |

## 2.2 Battery model

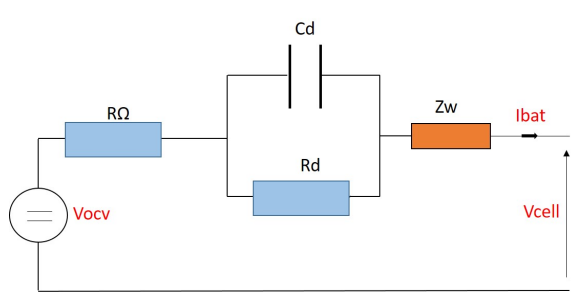


Figure 2-1: Randles model of a battery cell.

Modelling the behaviour of electrochemical power source is an important issue in simulation of systems. When modelling a electrochemical process, partial differential equations must be solved [8]. This pure mathematical model can be replaced by electrical models that has more relation between the model parameters and the battery behaviour. On top of that, heavy computational processing generated by mathematical models makes it less efficient in real time application [9] compare to electrical models. One of the most simple and common used electrical battery model is the randales model shown in fig.2-1 [10], [8].

The components of the model are:

- $V_{ocv}$**:** The voltage source of the equivalent circuit is the open circuit voltage, it means the voltage when the cell is disconnected and it is in repose. This voltage is also characterized as the voltage in discharge process at C/25 [3].

- $R_{\Omega}$**:** Every cell shows an ohmic resistance, which is due to the limited conductance of the contacts , the electrodes and the electrolyte [3]. This ohmic resistance will depends on the SOC and the SOH.

- $R_d$ and $C_d$: To characterize the transient response of the cell, a resistance and a capacitance are employed. This parallel RC circuit is commonly referred to as a ZARC element [10].

- $Z_w$**:** The most challenging component to identify is the Warburg impedance ($Z_w$). It represent the diffusion phenomena inside the cell and it depends on electrolyte area, concentration of electrons and the diffusion coefficient(D) [11]. This Diffusion phenomena describe the mass transfer through the electrodes and must be represented thanks to the second Fick's law (2.1)[12].

$$\frac{\partial X(x,t)}{\partial t} = D\frac{\partial X^2(x,t)}{\partial t} \tag{2.1}$$

  where X(x, t) is the electron concentration at the abscissa x and time t and D is the diffusion coefficient. However, it is agreed that the most suitable model for real time implementation of $Z_w$ could be a series of RC circuits fig.2-2 [12], [9],

[13]. In the Randles scheme, the Warburg impedance stands for the diffusion phenomenon and consequently represents the overpotential due to the species concentration [9].

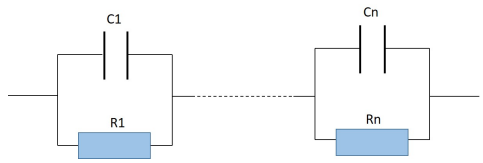


Figure 2-2: Electric equivalent circuit model of a warburg impedance.

Taking into account this assumptions the mathematical expression of the Warburg impedance is as follows:

$$Z_w = \sum_{i=1}^{n} \frac{R_i}{1 + R_i C_i s} \tag{2.2}$$

Hence, the total impedance of the Randles model becomes:

$$Z = R_\Omega + \frac{R_d}{1 + R_d C_d s} + Z_w \tag{2.3}$$

where s is the Laplace variable.

### 2.2.1 Parametrization

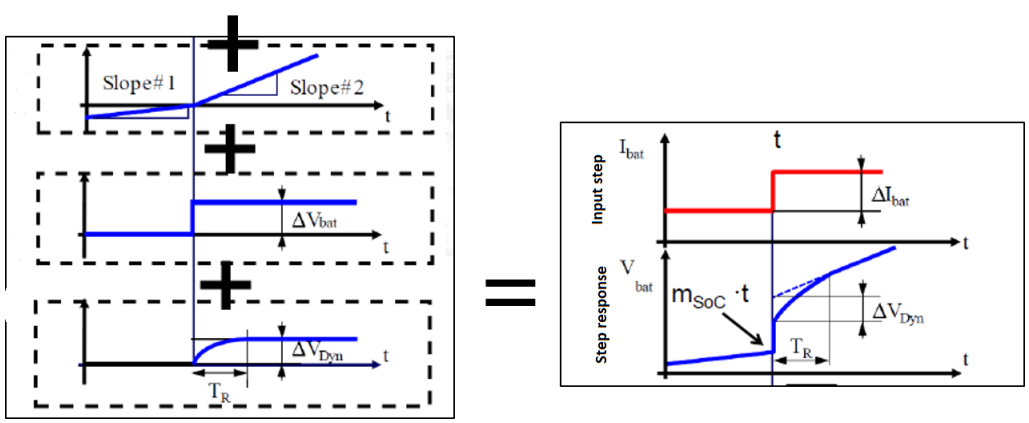


Figure 2-3: Measured the voltage response for the internal impedance.

The impedance parameter can be obtained by applying a current pulse and measuring the voltage response as it is shown in fig.3-8. With $\Delta I$ and $\Delta V$ the serial ohmic resistance $R_\omega$ can be estimated. $R_d$ is shown above.

$$R_d = \frac{V_{final}}{\Delta I} - R_\omega. \tag{2.4}$$

The dynamic capacitor is calculated from the time constant of the subsystem 3 3-8. In a first order system, the settling time can be approximated by three times the RC constant ($\tau$)

$$Ts = 3R_dC_d \tag{2.5}$$

Other method to calculate the parameters is the electrochemical impedance spectroscopy (EIS). This method consists in inject small ac current to the battery under test, measuring the ac voltage. The strategy permits to get impedances from low frequencies to high frequencies. Compared to step response method, small signal excitation allows for direct measurement and provides information in order to get Zw. For this purpose, it is very useful in battery studies at low frequency [10]. Fig.2-4,

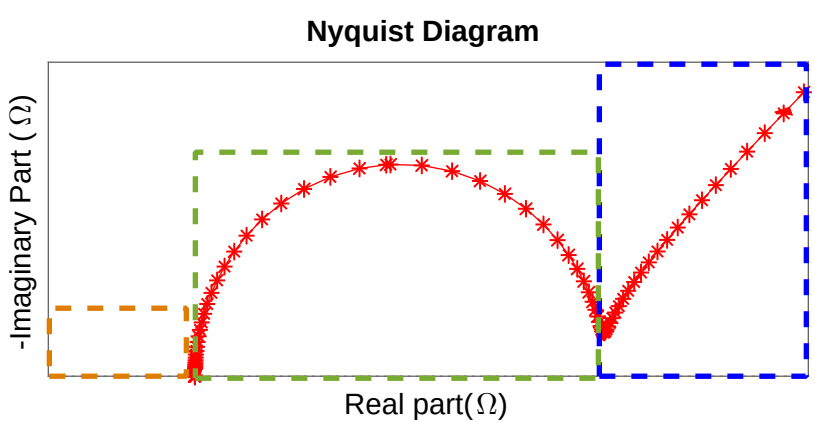


Figure 2-4: Ideal Nyquist plot of an internal cell impedance.

shows the ideal nyquist plot of an internal impedance for a cell battery. The x-axis and y-axis represent real and imaginary values of the internal impedance, respectively. The figure is delimited by rectangles each of them gives the necesesary information to get randles parameters. It is important to note, that only the capacitive behaviour of

a cell is ploted, it means that positive values of the reactance (inductive behaviour) are not shown in the plot as they are not use in the randles model fig.2-1. The ohmic resistance is inside the orange box fig.2-4, and it is identify as the value where the behaviour of the battery changes from capacitive to an inductive behaviour [14].The Rd-Cd parallel circuit in the Nyquist plot is defined as a semi-circle, where the tau constant of the circuit can be obtained from the minimium impedance value (the top value in the semicircle) [14], [13]. Low frequencies impedance values, inside the blue box, depicts the Zw.

## 2.3 Battery Management System

In this section a briefly description of a BMS is presented. Now a days the vast majority of battery manufacturers provides a BMS together with the battery.

### 2.3.1 The need for a BMS

As it was explained in previous chapters, a battery pack is made by a group of cells. Imbalance of these cells are very usual being internal reasons such as manufacturing variance in physical volume, variations in capacity and differences in self discharges [15]. This leads to either different internal resistance or capacity. Generally, the higher number of cycles, the higher unbalanced between cells [3]. Therefore, cells inside a pack, might be able to have different voltage each other, thus different SOC producing a waste of battery energy. On top of that, unbalanced between them leads to ageing cells, since there would be cells suffering either deep discharge or charge processes compare to their counterpart. Furthermore, temperature unbalanced are mainly provoked by these differences in voltage, internal resistance and capacity contributing to a lower life expecting. Therefore, it is clear the need for a energy management called battery management system when is applied to batteries the main function are measuring voltage, current and temperature. This not only controls the operational conditions but to prolong its life and guarantee its safety. A complete BMS module also provides accurate estimation of SOC and SOH for the energy management

module.

### 2.3.2 Equalization cells

Cells with reduced capacity or high internal impedance tend to have large voltage swings when charging and discharging. Then, it is necessary to cell balance, overall lithium chemistry, because of its overvoltage potential [16]. The issue is to equalize the voltage and the state of charge cell by cell. A briefly description would be to extract energy from a higher voltage cell(s) to let them either burn it in a dissipative element or injected to lower voltage cell(s). Therefore, there are two major categories in balance methods: passive and active methods [16][15].

Passive balance strategies works with passive elements such as resistance. The aim is to burn the excess of energy through them fig.2-5. This is is a simple method, easy to implement and it might be the cheapest one, however heat dissipation provokes lower effectiveness. Also uneven temperature between cells will aggravate the imbalance between them [4].

Active cell balance uses extra circuit to transfer the extra energy to the less highly charged cells. In many cases the active strategy is a complex method so a trade off bewtween the circuital complexity and achievable efficiency has to be found to make active balancing competitive against passive method. The equalization can be done either on-line, it means when the battery is working, or off-line that is to say the module or battery pack is disconnected from the whole pack. Different active balancing techniques are possible depending on how the energy is redistributed among the cells. In this master thesis, the classification is done according to the flow energy; battery-cell, cell to cell or cell to battery.

- **Cell-battery:** The technology is based in isolated DC DC converters. The strategy is transferred the energy form the highest voltage cell to the lowest voltage cell through a converter. The inputs of the converter are connected to each cell to be balanced. The outputs of the converter are connected together

and to the total battery pack. This method needs boost the voltage from the cell to the pack so its suitable for balancing battery modules when, there is no a big difference in voltage, otherwise a big converter is needed. The system is suitable when there is a huge number of cell(s) with an excess of energy and many converters can work simultaneously [15]. Fig.2-5(c).

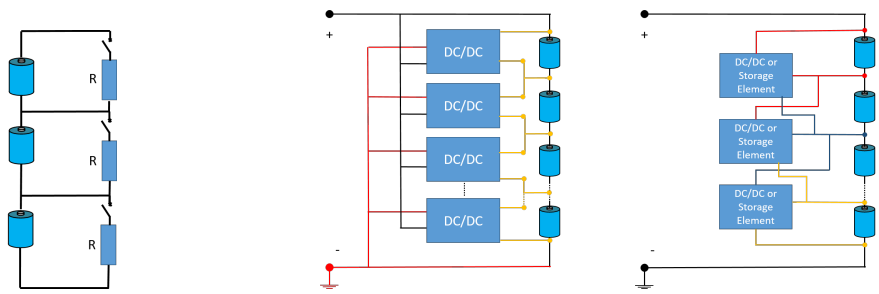


(a) Passive (b) battery to cell (c) cell to cell

Figure 2-5: Basic schematic for proposed boost buck converter

- **Battery-cell:** Similarly, than the previous one, it is a technology based on isolated DC-DC converters. These DC DC power electronics used for cell balancing fall into several categories such as: flyback, ramp or resonant converters [17] [16]. The higher the number of cells with lack of energy, the higher the converter efficiency. Both battery-cell and cell-battery can be bidirectional converters in such a case the energy can flow in both directions.

- **Cell-cell:** This balance method can use either isolated and non-isolated DC DC converter. The strategy is to extract the energy from the highest voltage cell and delivered it to the lowest voltage cell without passing the energy through the whole pack. The energy is going from cell to cell (switched method) or from the most charged to the lowest charged cell (distributed method). In any case a temporary energy storage device is needed, ususally capacitors , however an extra cell or module can be used. Many papers call this method shuttling active [15][16]. The basic topology switched capacitor uses a n-1 capacitor to balance n cells, its simple and it does not need control. The distributed method uses only one capacitor, higher number of switches and it requires control. The

disadvantage of cell to cell is the long time needed to equalize the battery. However it is a quite simple method, very cheap and it does not require any control. It would be a good option for balancing a huge number of cell where the system is always working. It can work in both charge and discharge process which is suitable in applications where the battery does not have a end of charge state.

- **Disconnected pack:**A battery module or a single cell can be disconnected from the charge process. This method is usually applied to modules, when a battery pack is overcharged , it means with an extra energy , it is by-passed from the path charging current, until the next pack are charging a the same level. Obviously, this will affect the battery efficiency, and it is a method used just during charching process. However, some applications allows to replace the module by another module in such a way there will be always an extra pack allowed [18]. This methodology provides an active balance method, fast and flexible. In contrast, it needs huge switches which must be able to interrupt high current values. In addition, losses due to conduction in the switch might be significant.

### 2.3.3 SOC and SOH estimation

As it was explained in the overview, the state of charge estimation in batteries are one of the main BMS task. A properly way of obtaining a SOC value leads to get a useful information in order to avoid battery degradation. The main methods fall into three major categories: direct measures, current integration and methods based on mathematical algorithms such as kalman filters.

- **Direct measurement method:** The Open Circuit Voltage (OCV), is directly related to the state of charge. A properly SOC estimation, the OCV measurement must be very stable. It implies that the battery cannot be neither in charge nor discharge process. This makes difficult the measure on-line.[19]. Another method is to measure the internal impedance. The internal impedance

Table 2.2: Cell balance. Comparing method

| | **Cell to battery** | **Battery to cell** | **Cell to cell** |
|---|---|---|---|
| **Type of converter** | Isolated DC DC<br>low to high voltage | Isolated DC DC<br>high to low voltage | Non isolated DC DC<br>low voltage, low Voltage |
| **Num. of Converters** | N | N | N-1 |
| **Direction and operation** | Fed by a cell when<br>it has excess of<br>charge<br>feeds the battery | Fed by the battery<br>Feeds a cell when<br>it has insufficiente<br>charge | Fed by the cell when it<br>has higher voltage than<br>the adjacent cell |
| | | | |
| **Pros** | More efficient::high<br>voltage output<br>rectifiers<br>Simpler: low voltage<br>transistors controlled<br>from same low voltage<br>side as the cell electronics<br>Fastest balancing when<br>the majority of converters<br>are operating | Fastest balancing<br>when most cells<br>are low: the majority<br>of converters are<br>operating | Fewer converters<br>Simpler, cheaper solution<br>DC DC at low voltage |
| | | | |
| **Cons** | Expensive, big converters | High voltage transistor<br>Requires isolated con<br>trol from cell electronics<br>(low voltage side)<br>to drive transistors( High<br>voltage side).<br>complex, expensive | More wires<br>takes longer to balance<br>Overall efficiency quite<br>lower than other.<br>Losses occurs at each<br>step. |
| | | | |

(IR), is also related to the SOC, it can be obained injected sinusoidal currents to the battery and measuring the voltage [10]. The direct measure methods have the disadvantage of the impossible on-line measures.

- **Current integration:** This method is based on the current integration along the time eq.(2.6). It is a simple method, however it requires a very precise current measure [20]. In practice, the use of this method results limited due to its accumulative errors.

$$SOC(t) = SOC(t_0) - \int_{t}^{t_0} \frac{1}{C} i(t) dt \tag{2.6}$$

- **Kalman filter:** This methodology does not require a very precise measurements, but it requires a very accurate battery models. As the battery is non-linear system, it involves complex mathematical algorithms and it just provides an estimation [21][22]. The main advantage is the online recognition.

Combined along the SOC estimation, a state of health estimation (SOH) is usually given, when a deeply analysis of battery state is done. SOH is very related to the ageing of cells. Many studies provides the next equation to define the SOH in cells along the time [4].

$$SOH(\%) = \frac{Q_a}{Q_r} x100 \tag{2.7}$$

where $Q_a$ is the initial nominal capacity cell and $Q_r$ is its actual capacity.

Table 2.3: SOC estimation methods.

| **Method** | **Characteristics** | **Requirements** | **Advantage** | **Disadvantage** | |
|---|---|---|---|---|---|
| **OCV** | Estimation through the | Very precise measure | Simple method | Battery disconnected | |
| | | | | | |
| **Coulumb counting** | SOC esitmation using the capicity values Ah | Very precise current measurement | Simple method | Bad estimation due to acumulative errors | |
| | | | | | |
| **Internal resistance** | SOC estimation from internal resistance | Special equipment EIS electrical impedance Spectroscopy of converters are | Simple method | Expensive equipment Off-line | |
| | | | | | |
| **Kalman filter** | Mathematical methods models to estimate the SOC | Current , voltage and temperature measurement | SOC Estimation quite precise. Online measurement. lower than other. Losses occurs at each step. | Complex mathematical models. | |
| | | | | | o |

### 2.3.4 Architecture

Attending at the architecture, a BMS can be: flat or modular [1]. In the former, a single control unit is responsible for monitoring and controlling all cells. This is a economic solution and might be applicable when lower number of cells are controlled. However, the architecture is not scalable and might be complex when high number of components. By contrast, a modular architecture controls a package of cells reducing wires and complexity. Such a distributed scheme makes monitoring more efficient, and

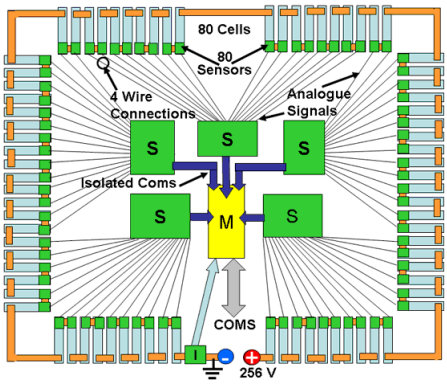


Figure 2-6: Modular architecture [1].

energy-efficiency higher than the flat architecture. However, the cost of components increases. Fig.2-6.

### 2.3.5 Review BMS technology

Here a briefly review about the technology used for BMS equalization cells is presented.

#### 2.3.5.1 Shunting dissipative balance method

This method is used by the 80% of the equalization cell(s) [23]. It removes the excess energy from the higher voltage cell to a dissipative element. The popularity of this method is its simplicity and costless. It can be divided into two categories fixed shunt resistor and switched resistor fig.2-5. The former uses continuos bypassing current for the all cells and the resistor is adjusted to limit the cells voltage. It can ne only used for Lead -acid and Nickel based batteries because they can support overcharge conditions for a while [16]. The switched resistor(SR) consists in a switcher to baypass the highest voltage cell as it is shown in fig.2-5. The advantage for these methods is that it is not used complex control methods, and it is cheap, however in SR method voltage monitors are added to each cell make it expansive when huge amount of cell must be balanced. The disadvantage are slow balance technology, low efficient and thermal problems.

#### 2.3.5.2 Capacitive shuttling balancing method

This method basically utilize capacitors as external energy storage elements for shuttling the energy between the cells. The capacitor shuttling can be divided into three configurations: switched capacitor, double-tiered switched capacitor and single switched capacitor [24]. The basic idea of a switched capacitor is shown in fig.2-7. In this topology to balance n cells 2n switches and n-1 capacitors are required. The

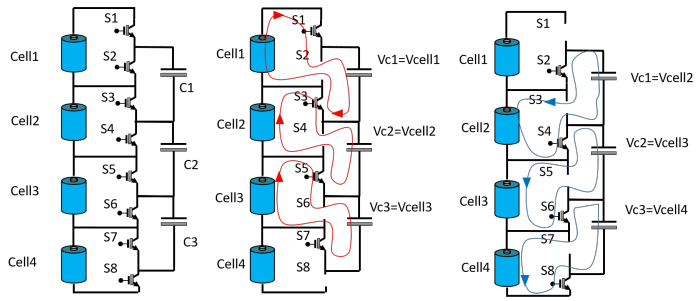


Figure 2-7: Switched capacitor topology.

control strategy is very simple because there is not control the switches work with the same duty cycle but in complementary mode as it can be seen in the figure. Hence, there are only two states. For instance in one state $C_1$ is paralleled wtih cell $cell_1$ and the capacitor is charged or discharged to obtain the same voltage that the cell. Then in the rest half period , the same capacitor ($C_1$) will be paralleled with the adjacent cell $cell_2$ and the same phenomena will happen at this state. After cycles of this process it is expected that both cells voltage are equal each other. The advantage of this method is that it does not need neither control nor voltage sensor. Nevertherless, it is a slow balance method. The single switched capacitor can consider as a derivation of the Switched Capacitor, but it uses only one capacitor. It drastically reduce the number of these components, however it needs a complex switches network. in fact it needs n+5 number of switches to balance n cells. As an advantage compare to the previous one is that with the appropriate control the time of balance can be improve. The doubled-tired switched capacitor is also a derivation of the basic structure. The advantage is that the second capacitor fig.2-8 tier reduces the balancing time to a quarter of the time needed for the switched capacitor method. In addition, the

capacitor-based topologies can work in both recharging and discharging operation.

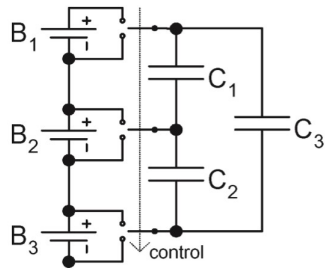


Figure 2-8: Doubled tiered switched capacitor topology.

#### 2.3.5.3 Buck-boost balancing method

The scheme proposed in here is based on the buck boost converter topology, for balancing one cell a 2n switches are needed and just one inductor. These method is widely used and it has several balancing topologies [16][15] [17]. When the duty cycle is less than 0.5, the circuit operates in the buck mode. On the contrary, when the

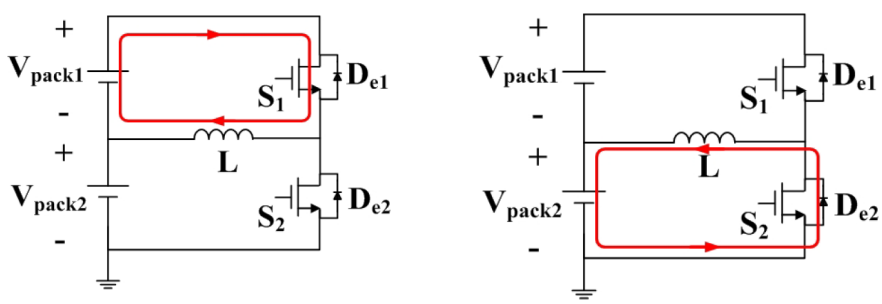


(a) V1>V2 first half period (b) V1>V2 second half period

Figure 2-9: Basic schematic for proposed boost buck converter

duty cycle is greater than 0.5, the circuit operates in the boost mode. By fluctuation of these two the switches, the energy can flow in both directions. Fig.2-9 shows the basic schematic. In this first state when the voltage in the battery pack or cell 1 is greater than the voltage in cell(s)2 the swhitch S1 and the body diode of the S2 will be turned on and the energy of the battery is transferred from cell1 to cell2. Similarly, when the voltage is reversed, the switch S2 and the free whiling diode of switch S1

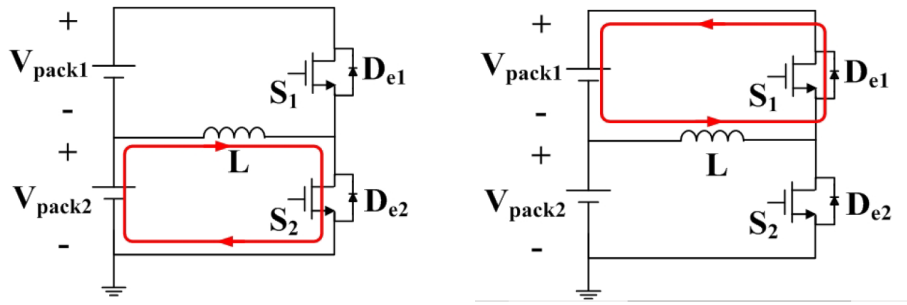


(a) V2>V1 first half period (b) V2>V1 second half period

Figure 2-10: Basic schematic for proposed boost buck converter

will be turned on fig.2-10. The system just requires one passive element , and two switches that might be high power switches in the case to balance packs instead of cells. The system presents better efficiency compared to shuttling capacitor balance , however voltage sensing and an intelligent controller are needed, making the system more expensive.

#### 2.3.5.4 Flyback converter balancing method

Flyback converters are used in isolated structure and they can be unidirectional or bidirectional. The basic principle is that the most energy cell is stored in the inductor

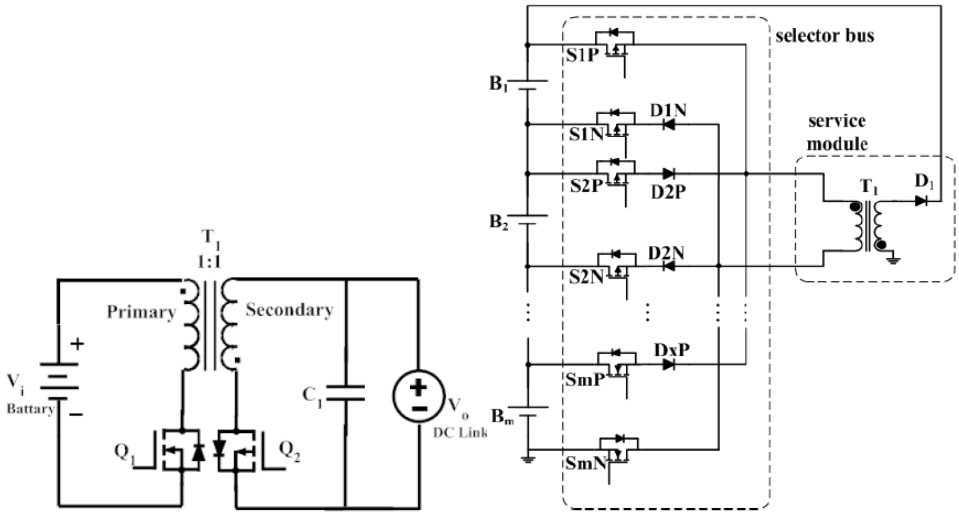


(a) Transformer charge (b) Transformer discharge

Figure 2-11: Flyback converter topology [2].

coupling flyback converter and then released to the lowest cell. For instance if V1 in fig.2-11(a) is overcharged, Q1 receives a digital signal an the energy will be released to the primary magnetic coupling. This topology is fully explained in [2]. Fig.2-11(b) shows an example of one proposed balancing circuit using a flyback [2]. By sensing the voltage and the SOC of each cell or pack they will be connected through a bus selector (2n Switche) to the flyback converter which can be connected to the whole pack or to an external voltage source energy. The use of flyback is morte flexible in energy transmission since the energy can be transferred from the pack to the cell ( bidirectional converter). As advantage it is an isolated converter, with low current ripple which is good for batteries. Drawbacks are the magnetic losses, complex control and low efficiency converter (80%).

#### 2.3.5.5 Multiwinding transformer

Multi-winding transformers are also used in battery cell energy flow. It consists in a single primary winding with secondary taps for each cell fig.2-12. Current from the battery pack is switched into the transformer primary winding and induces currents in each secundary. The switcher can be a controlled device, it requires control to make the decision about what switch must be on or it can be just a diode, in such a case the secondary with least reluctance will have the most induced current.[17].


(a) Transformer charge (b) Transformer discharge

Figure 2-12: Battery cell active method. Multiwinding transformer.

### 2.3.6 Comparative analysis

Table 2.4: Comparative analysis balance topology

| Scheme | Advantage and components | Disadvantage | |
|---|---|---|---|
| **Switched resistor** | Cheap , simple , fast equalization<br>n resistor, n cells | Not very effective, high energy losses ,<br>thermal management problems , high resistors | |
| | | | |
| **Switched capacitor** | No control, charging and discharging process<br>low voltage stress, relatively cheap, different topology<br>2n switches, n-1 capacitor (basic) | Low equalization rate, many switches<br>Control depending on topology<br>medium efficiency. | |
| | | | |
| **Single inductor Buck- boost** | Fast equalization speed,<br>Good efficiency, 1 inductor, 2n switches, n-1 cap. | Complex control, switching current stress<br>Filtering capacitors for high switching currents | |
| | | | |
| **Multi-inductor Buck-boost** | Fast equalization speed, good efficiency<br>Good efficiency, 2(n-1) switches<br>and the same number of diodes , n inductors | Less Complex control, accurate voltage sensing<br>switches stress, charging mode only | |
| | | | |
| **Multiwinding transformer** | Fast balance, very robust , no complex control, high efficiency<br>Low current ripple to the battery, isolated converter<br>1 trafo, n windings, n inductors, 2n capacitor, n switches | Magnetic losses, needs control, high cost<br>not very scalable. | |
| | | | |
| **Flyback** | Isolated, low current ripple, depending on topology | Low efficiency, usually unidirectional,<br>magnetic core losses, needs control | |
| | | | |

A comparative chart of equalization methods is shown in table.2.4.Among of these methods it is clear that the decision to chose one topology or another normally depends on the application. Fig.2-13 shows the LiFePO4 racks used in the project. The

Figure 2-13: Whole battery pack. 15 modules of 255 LiFePO4 cells each.

idea is to develop a dual balancing method, one to balance modules (racks) and the other one to equalize cells inside a module. The former one is out of this master thesis

scope however, a briefly description about the method used is explained below. As it was stated in the introduction chapter, the battery is 15 racks and each one consist of 255 cells, shaping a 15x15 configuration. If a system of balancing rack to rack wants to be implemented, an exhaustive study about the power management must to be done. It is clear that a passive implementation should never be chosen not only for its lower efficiency but its longer time to balance. So the decision is to select, an active method. Each cell is 3.2V and 3200mAh , so the power manage will be 48Ah and 48V per rack. According to this, a good efficiency converter must be used. Flyback converters, presents poor efficiency so topologies based on this converter are rejected. The system must be fast, so switched capacitor topologies should be discarded. In this project, a dual active bridge converter (DAB) is finally decided to be the power topology. Taking into account the power flow, the equalization method is from cell to cell or in this case form module to module. The system can be done to fault tolerant method, in such a case an extra cell or module must be introduce fig.2-14.

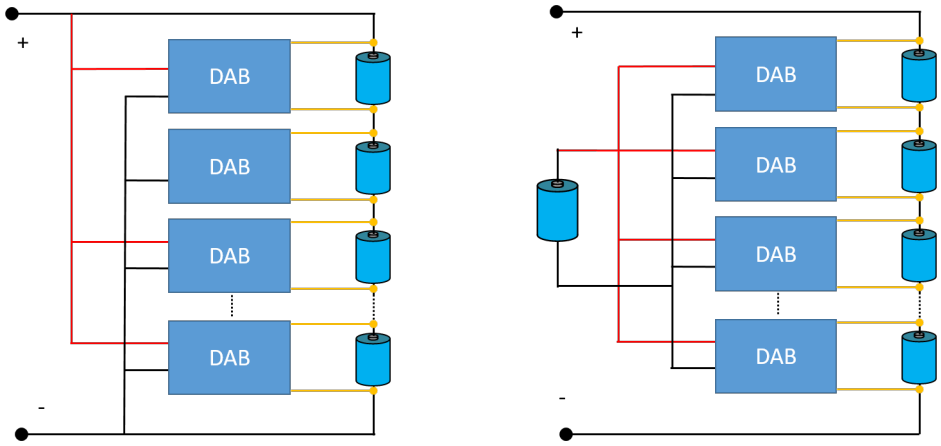


(a) Pack to pack equalization method (b) Fault tolerant equalization

Figure 2-14: Module active equalization scheme using DAB.

This additional pack might not have the same power than the rest of modules, therefore it made from a lower number of cells. reducing. The topology decision was made based on the benefits of the converter. A DAB is built of a two H bridge converters connected through high frequency transformer fig.2-15. The leakage inductance and the magnetic inductance of the transformer is in charge of the energy transferred

between modules. It is a bidirectional converter that has a good dynamic response so it provides a very fast balance. Once the active balance method is decided to

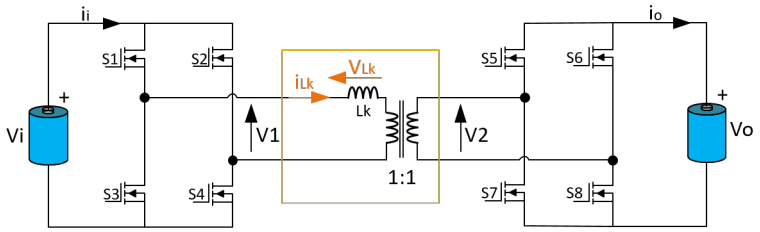


Figure 2-15: Dual active bridge.

equalize modules. The second part is to balance cells inside a module. In this master thesis, a balance method at level cell, has been design, simulated and implemented in the lab. Normally dissipative methods are good for low power application, when the resistor is small and it does not need so much thermal management. Due to its simplicity and cheap implementation it is very popular however when high number of cells must be balance measuring cell voltage, makes the system more expensive. The use of converters for each cell, it would be a complex method due to the control and very expensive because the high number of cells. Based on this, the use of switched capacitor is a good option according to the requirements. It can work in either charging or discharging process, it is simple to install and it does not need any control.

# Chapter 3

# Dynamic battery model

As stated in chapter one this thesis is part of a real project based on a large scale EEES connected to a micro-grid. It is important to remark that batteries will be either absorbing or delivering energy continuously. In these applications several difficulties arise [10]: (I) batteries are not stationary, (II)electrochemical systems are highly non-linear systems and these non linearity is significant for many design systems, (III) the dynamical behaviour depends on many parameters like temperature, SOC, current rate, etc. The aim of this part is, to obtain knowledge about battery

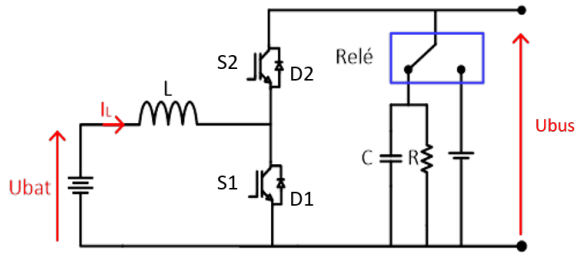


Figure 3-1: DC DC bidirectional converter scaled in the lab.

performance under different working operation points. To reach this goal a scale DC DC bidirectional converter has been developed in the lab. Fig.3-5 shows the scheme. It makes an exact copy of the converter utilized in the real project fig.1-1. The interleaved inductance is replaced by a single inductance and the three phase legs is changed by a single phase. Obviously, rather than study the behaviour of a seven module of 255 cells each, the converter just studies the operation of a single cell.

Further researchers, could demonstrate if these results obtained from a cell's level might be extrapolate to a whole cell's pack.

The DC DC converter works at 15kHz. The internal impedance cell is unknown at that frequency and this could be a problem working with other system elements due to resonance phenomena. The converter allows us charging and discharging cells at different current rates and SOC and see how the internal impedance varies at different frequencies. Taking advantage of the commutation harmonics, we can get impedance values at multiples of the switching frequency. This will help control designers to have knowledge about plant models in order to tune regulators and draw filters such as LCL, or LC without resonance problems.

## 3.1 DC DC converter

The topology is a bidirectional converter. The input voltage is the cell voltage (Ubatt) fig.3-5 and the Vo is the bus voltage. When the battery is discharging the topology is working as a boost and the energy is burnt it through a resistance. Additionally, it is possible to connect a 24V DC source in such a way the converter works as a buck converter and the battery is charged. In both cases, the current is controlled.

### 3.1.1 Operation principle

MOSFET S1 and S2 operate in complementary mode and between them there must be a dead time in order to avoid short-circuit leg. The delay between them, is produced by software. A PWM signals is generated by a microcontroller. In boost operation mode the energy is flowing from the battery to the load, when S1 is open the inductance is charged, the voltage drop in the element equals to the battery voltage and the output capacitor voltage proportionates the output voltage fig.3-2(a). When S1 turns off, the energy storage in the inductor is discharged to the load through a body diode D2. It is the completely boost converter mode, steady state equations are depicted below. This operation is applied to evaluate the battery cell behaviour

in discharged mode.

- **S1 on:**

$$V_L = L\frac{dI_L}{dt} = V_{bat} \tag{3.1}$$

$$V_C = -V_o \tag{3.2}$$

$$\Delta I_L = \frac{DT}{L}V_{bat} \tag{3.3}$$

- **S1 off:**

$$V_{bat} - V_o = L\frac{dI_L}{dt} \tag{3.4}$$

$$\Delta I_L = \frac{(V_{bat} - V_o)(1-D)T}{L} \tag{3.5}$$

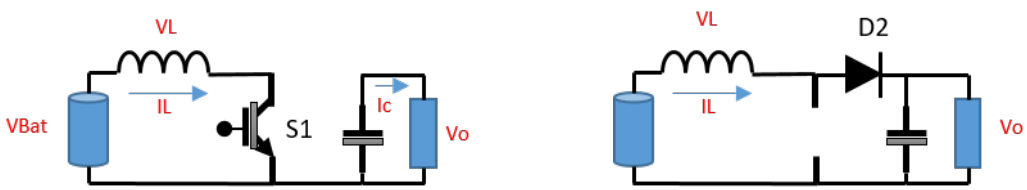


(a) Boost S1 on: (b) Boost S1 off:

Figure 3-2: Boost operation mode.

The inductor current has to be the same in steady state so combaining eq.(3.3) and (3.5) the overall change in the current must be zero. Hence, the duty cycle:

$$D_{boost} = 1 - \frac{V_{bat}}{Vo} \tag{3.6}$$

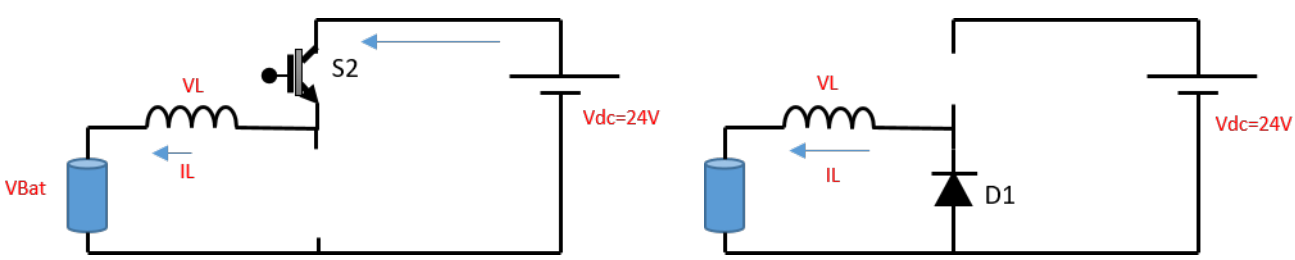


(a) Buck S2 on. (b) Buck S2 off.

Figure 3-3: Buck operation mode.

Moving on to the buck operation mode, the power is transferred from the 24 volts DC source to the battery cell. When S2 is conducting and S1 is open, D2 is reversed bias and the inductor current is charged linearly. The voltage drop is the different between the DC source and the cell voltage. The next part of the period, S2 is closed and the inductor current continues to flow through the body diode D1. Similarly than before this operation mode permits to have knowledge about the cell's behaviour when it is charging. Fig.3-3 shows the buck operation mode and mathematical expression are shown below.

- **S2 on:**

$$V_L = L\frac{dI_L}{dt} = Vdc - Vbat \tag{3.7}$$

$$\Delta I_L = \frac{Vdc - Vo}{L}DT \tag{3.8}$$

- **S2 off:**

$$V_L = -Vbatt \tag{3.9}$$

$$\Delta I_L = \frac{-V_o}{L}(1 - D)T \tag{3.10}$$

As it was explained previously if we assume that the converter operates in the steady state, the energy stored in each component at the end of a commutation cycle T is equal to that at the beginning of the cycle. Combining equations (3.8) and (3.10) the duty cycle is:

$$D = \frac{V_{dc}}{V_{bat}} \tag{3.11}$$

### 3.1.2 Converter design

Four parameters are established to calculate the power stage circuit: input voltage (Vin), output voltage (vout), maximum output current ripple ($\Delta I$) and maximum output voltage ripple ($\Delta V$). The selecting parameters are chosen according to the two operation modes, buck converter and boost converter. Table.3.1 indicates the operating parameters. The voltage ripple is not so a key issue because the bus voltage is not so important in order to study the cell behaviour. However the current ripple

is determined carefully, because large ripple is supposed to damage the battery but lower ripple will never allow us to get knowledge in high frequency behaviour. In both cases the maximum current is set up as 2C (6400mAh). After selecting the operating

Table 3.1: Operating parameters

| **Parameter** | **Value** |
|---|---|
| $V_{in}$ boost | 3.2V |
| $V_{out}$ boost | 24V |
| $V_{in}$ buck | 24V |
| $V_{out}$ buck | 3.2V |
| $\Delta V$ | 0.4V |
| $\Delta I$ | 10% |

working points, we calculate the minimum duty cycle for buck mode and maximum duty cycle for boost mode, applying equation (3.11) and (3.6), respectively. The converter should always work under these limits. The inductor selection is computed according to the desired current ripple, and the switching frequency for both operation points. Then, the largest value is selected considering that requirements would be covered in both operation modes. They are calculated from equations [25].

$$L_{buck} = \frac{V_{out}(V_{in} - V_{out})}{\Delta I F_{sw} V_{in} I_{out}} \tag{3.12}$$

where $V_{out}$ is the nominal cell voltage, vin is the DC source 24V, the switchiog frequency is $15kHz$, $\Delta I$ is the current ripple and $I_{out}$ should be the maximum charging current 1C establish by the manufacturer. In this case the value has been oversized to let charging current at higher C.

$$L_{boost} = \frac{Vin^2(V_{out} - V_{in})}{f_{sw} \Delta I I_{out} V_{out}} \tag{3.13}$$

For the L boost calculation the dimensioned parameters are the same. The largest value is given in buck mode and the L inductor is $425\mu H$. notice than in boost mode the output parameters operating points are not important because neither output voltage nor output current are controlled. The output capacitor value is calculated

from eq.3.14 [25].

$$C_{out} = \frac{I_{out} D_{boost}}{f_{sw} \Delta V} \tag{3.14}$$

where $I_{out}$ is the maximum current desired in this case related to the maximum inductor current value which is 6.4A $I_{out}$=$I_L$(1-D), and $\Delta V$ is the output ripple voltage. Hence, $C_{out}$=1000$\mu$F.

### 3.1.3 Inductor design

The inductor design is fully explained in [26]. The equivalent toroid method is used to design and make the inductor. The wire is a 0.65mm Cu, and the material core is Fe-Si-Al made from alloy powders of iron, silicon and aluminum. A brief physics explanation comes next. When a current is circulating in a number of turns fig.3-4, a magnetic field intensity H is created as reported by Ampers law (3.15) [26].

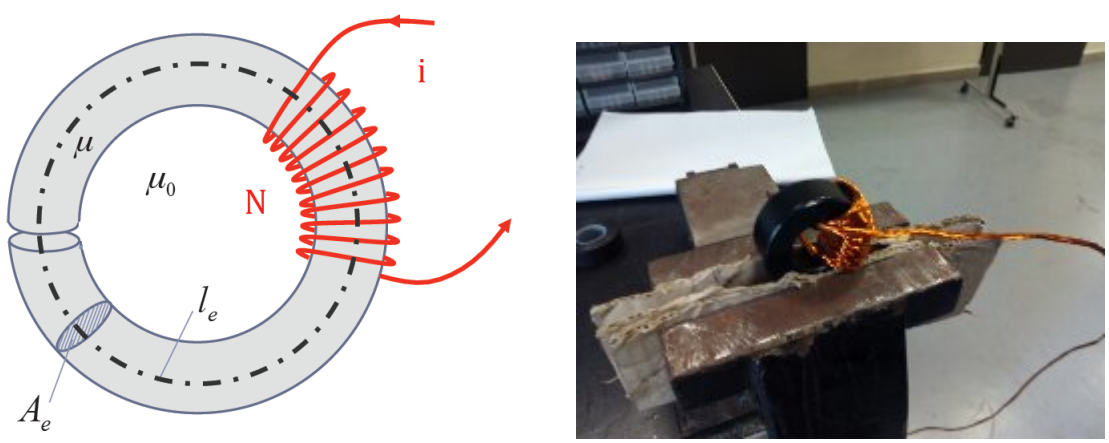


(a) Theoretical torid with a N number of turns (b) Fabrication process of the inductor

Figure 3-4: Toroid equivalent method.

$$H = \frac{Ni}{l_e} \tag{3.15}$$

This equation represents the flux intensity for a given core geometry without air gap. The magnetic permeability coefficient ($\mu_o \mu_r$) depends on the given material and it correlates the flux intensity with flux density (B),(3.16). From B and knowing the geometry used, the magnetic flux is obtained (3.17). It gives an idea of the overall

energy stored in a magnetic volume.

$$B = \mu H \tag{3.16}$$

$$\phi = BA_e \tag{3.17}$$

hence,

$$\phi = \frac{\mu_o \mu_r A_e N i}{l_e} \tag{3.18}$$

According to $Faraday's$ and $Lenz's$ law (3.19), a flux variation over the time induces a voltage in a coil, the negative values is due to the voltage effect opposes the phenomena that induced it. The inductance L relates the current and the voltage in a given winding in a magnetic circuit. Thus, the behaviour of the magnetic circuit can be modelled in terms of an electric circuit (3.20). If the flux is multiply by the number of turns, it obtains the so-called flux linkage ($\lambda$)[27], it is the flux link by the coal and it is related to the magnetic inductance (3.21).

$$e = -\frac{d\phi}{dt} \tag{3.19}$$

$$e = L\frac{di}{dt} \tag{3.20}$$

$$\lambda = N\phi = Li \tag{3.21}$$

By combining previous equation (3.21) and (3.18), we obtain the inductance value function of the geometry, the number of turns and the material properties (3.22).

$$L = \frac{\mu_o \mu_r A_e N^2}{l_e} \tag{3.22}$$

Therefore, by adjusting the number of turns the inductance value is procured. The effective area and length as well as the magnetic permeability coefficient are obtained by the datasheet manufacturer. Other important parameter to take into account is the saturation. Magnetic materials have an intrinsic limitations of the magnetic flux density. It means, that at the point of increasing current the magnetic flux

intensity increases (H), but it does not imply increasing the magnetic density (B). This maximum value is limited for a given material and it is extracted from the data sheet manufacturer. Table.3.2, summarizes the inductor parameter. The core losses and the joule losses has not be take into account as the efficiency of the converter are not a key point.

Table 3.2: Inductance parameter

| **Inductor** | |
|---|---|
| Turns | 60 |
| 4 Cu parallel wire | 0.65mm |
| Core | CS467060 |
| Efficiency | 97% |
| Winding factor | 45 |
| L | 490uH |
| $R_L$ | 0.42Ω |
| $f_{sw}$ | 15kHz |

### 3.1.4 Current control and matlab simulation

To check the proper circuit behaviour, a matlab simulation has been done in agreement with the calculated parameters. The battery is simulated as a ideal voltage source, the switches are ideal , the output resistance is selected as 24Ω 25W. The inductance and capacitor value are those calculated previously.

The aim of a matlab model is to develop the current controller of the circuit. As it was explained before the current cell must be controlled at any time in both process charge and discharge. A general proportional integral controller is used PI for the current control loop, being Kp the proportional gain and Ti the integral action (3.23). A PI regulator has an infinite gain in open loop at 0Hz frequency. The integral term will not stop changing until its input is zero and therefore if the system reaches a stable steady state, the error signal of the integrator will be zero. [28].

$$PI = K_p \frac{(s + \frac{1}{Ti})}{s} \tag{3.23}$$

In order to tune a PI regulator, a plant model must be establish. In this case, the

boost inductance is the first order system plant G(s)(3.24), and the close loop transfer function is the one from (3.25). Fig. shows the diagram block.

$$\frac{1}{Ls+R} \tag{3.24}$$

$$Tf = \frac{C(s)G(s)}{1+C(s)G(s)} \tag{3.25}$$

A popular tuning method consist on cancelling the pole with the controller zero,

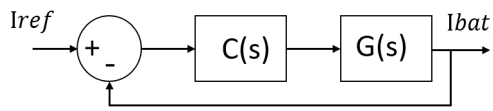


Figure 3-5: Block diagram of the current control loop.

while the proportional gain controls the system bandwidth. According to (3.24), the pole plant is located at $\frac{-R}{L}$, then the zero controller must be located over it. the Pi controller can be rewrote as in (3.26) The proportional constants are depicted in (3.27) and (3.28).

$$PI = k_p \frac{(s+\frac{k_i}{k_p})}{s} \tag{3.26}$$

$$K_p = 2\pi B_w L \tag{3.27}$$

$$\frac{K_i}{K_p} = \frac{R}{L} \tag{3.28}$$

where, $B_w$ is the desired bandwidth of the system ($100Hz$), L is the inductor value and R is the resistive part of the boost inductance ($R_L$). Although the output of a PI controller has no physical meaning, considering the characteristics of the system, what we are really controlling is the current through the inductor. Therefore, the input of the regulator is the error between the reference current and measured current and the output is the voltage drop across the inductor ($V_L$) .

Taking into account this, what we need is to get the voltage converter or ($V_{sw}$)().From $Vsw$ the duty cycle is easily obtained considering the mathematical equation (3.30). This duty is the needed for the PWM. Fig.3-6 shows the current control loop for the

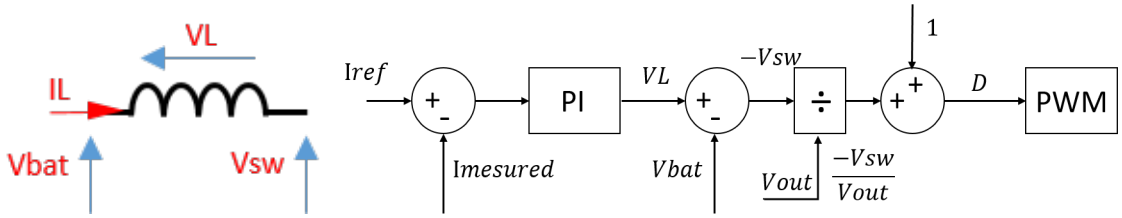


(a) $V_L$ (b) Controller block diagram .

Figure 3-6: Boost converter current control loop.

boost converter.

$$-V_{sw} = V_L - V_{bat} \tag{3.29}$$

$$D_{boost} = 1 - \frac{V_{sw}}{V_{bat}} \tag{3.30}$$

As the circuit is bidirectional converter, when the 24V DC source is connected, teh topology moves to buck mode. In such case the control must change, however the philosophy is the same, the output of the controller is the drop inductance voltage and the feedforward terms are introduced. Notice that if these feedforward terms are not introduce the system will work anyway, however the systems dynamics are much more improved in the case that the forward terms are added. The current close loop control when the circuit is operating in buck mode can be seen in fig.3-7 Fig.3-8

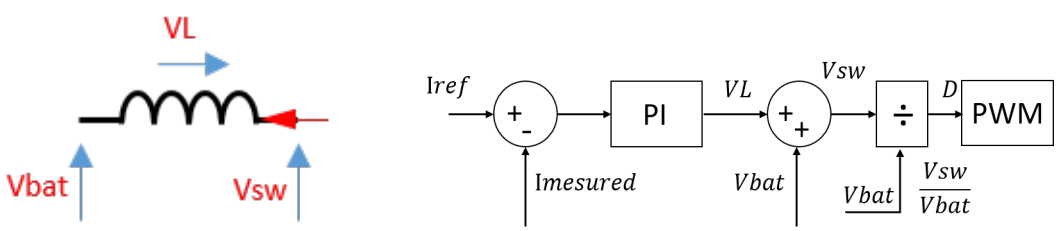


(a) $V_L$ (b) Controller block diagram .

Figure 3-7: Buck converter current control loop.

presents the simulation results done in matlab&Simulink. The graph shows tan step variation in current reference from 0 current to 2C. As one can appreciate the steady step error is 0 between the measured current in the inductor and the reference. The ripple is the one expected 10% more or less. The higher the ripple current, the higher amplitude in the harmonic content and therefore better for obtaining high frequency

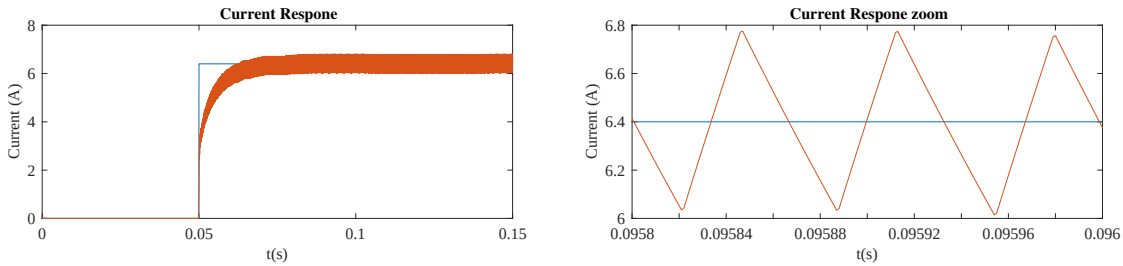


(a) Current response (b) Battery current ripple

Figure 3-8: DC DC converter current response simulation.

impedance.

### 3.1.5 Lab implementation

Once the converter has been design and simulated, the next setp was its implementation in the lab. For the design the Altium software has been used. The components has been selected attending the requirements considering current, voltage and power limits. The switches are MOSFET, the DC bus are made with an electrolytic capacitor place in parallel with a ceramic capcitor for high frequency ripple. A rele is in charged to switch between the output resistance (boost mode) and the 24V DC sources (buck mode) fig.3-5. A driver is selected to trigger switches, it is able to trigger 2 swithes. The dead time between signals, can be made by means of hardware or software. For control signals an external microcontroller F28335 texas instrument is utilized. The current is measured with a current trasducer LA55-P, and the DC voltage and battery voltage is collected by a simple voltage divider (3.31).

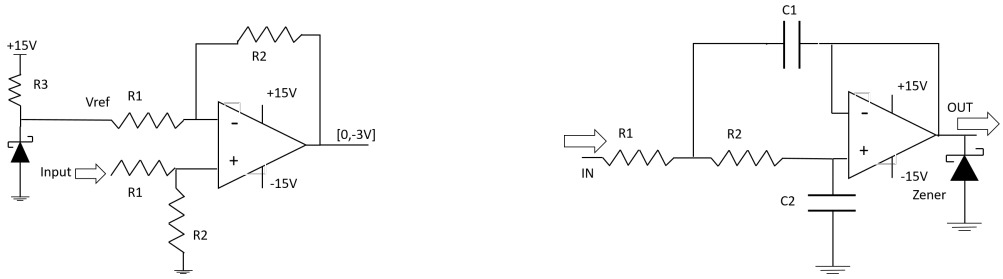


(a) Conditioning signal (b) Sallen key filter scheme

Figure 3-9: A)Conditioning stage, B)Filter stage.

To developed the current controller explained previously, the current must be measured and sent to the microcontroller. The LEM sensor provides current between (±50)A and this value must be adapted to the micro input range [0-3V]. This signal adapter is made by means of hardware. A differential OP amplifier circuit is used as it can be seen in fig.3-9(a). the equation that rules this operational amplifier circuit can be seen in (3.32).

$$V_{out} = V_{in}\frac{R2}{R1 + R2} \tag{3.31}$$

$$U_o = mU_i + b \tag{3.32}$$

where m and b are defined as:

$$m = \frac{R_2}{R_1} \tag{3.33}$$

$$b = \frac{R_2}{R_1}V_{ref} \tag{3.34}$$

The reference is utilized to shift the signals and the relation $\frac{R_1}{R_2}$ to adjust them to a proper value. Table.3.3 collects the electronic components for the adapter stage. Notice that in every single voltage supply Vcc and ground within a PCB, ceramic capacitors are added for filtering noise. After an adapter stage, the current signal

Table 3.3: Adapter circuit components

| **Component** | **Value** |
|---|---|
| R2 | 2kΩ |
| R1 | 1kΩ |
| $C_{vcc}$ | 100nF |
| $C_{gnd}$ | 100nF |
| OP | TL082 |
| R3 | 3kΩ |
| Zener | 3V |

Table 3.4: Bessel filter components

| **Component** | **Value** |
|---|---|
| R1 | 1.5kΩ |
| R2 | 1.5kΩ |
| R3 | 1.5kΩ |
| R4 | 47 |
| $C_{vcc}$ | 100nF |
| $C_{gnd}$ | 100nF |
| OP | TL082 |
| C1 | 27nF |
| C2 | 10nF |
| Zener | 3V |

must be filtered before sending to the microcontroller. A Bessel filter is selected fig.3-9(b). It is a second order filter, the cut off frequency is 8kHz and the filter components has been selected using webench filter design of texas instrument. Table.3.4 shows

Table 3.5: Converter components

| **Component** | **Characteristics** |
|---|---|
| power MOSFET | IRFZ24 $V_{ds} = 60V$ $V_{gs} = 10V$ $R_{ds}$=0.10Ω |
| Driver | ST LA6392 |
| Rele | 5V Omron |
| Current sensor | LEM LA-55P |
| External inductor | 496uH |
| Electrolytic capacitor (bus) | 1000uF |

the components used in the filter stage. In the filter scheme a zener diode is also used to protect the device against overvoltages. fig.3-10 summarize the different stages of

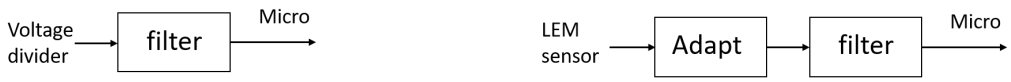


(a) Current signal (b) Voltage signal

Figure 3-10: Adapter and filter signal.

the signal process. These data will be finally sent to the analalog to digital converter module of the microcontroller. Te rest of the components of the DC DC converter are summarize in table.3.5. To these components an interrupter and a led ha been placed in the PCB for only connect or disconnected pulses.

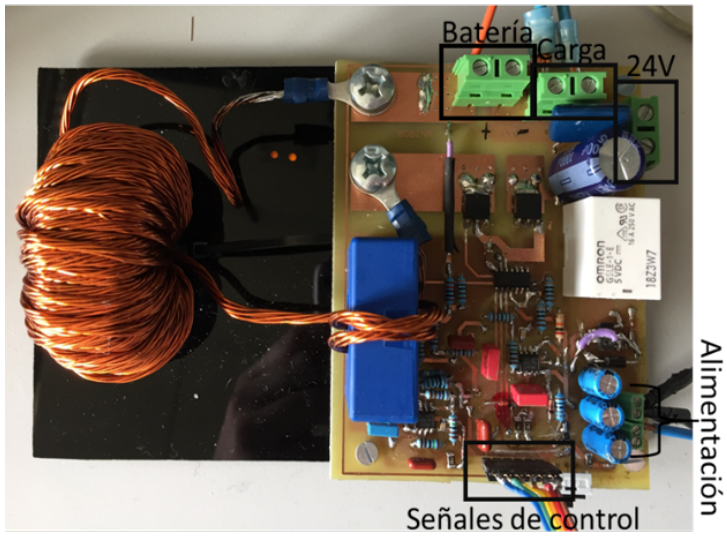


Figure 3-11: Bidirectional converter.

### 3.1.6 ADC converter and digital control

Since signals have been processed as explained before, the next step is to implement a digital control. To do this, an analog digital converter (ADC) is used, one channel for each parameter. The F28335 microcontroller has 16 ADC channels of 12 bits. This device will sample physical variables such as current battery, voltage battery and bus voltage and converts them into a binary number in this case 12 bits. The continuous function in Laplace time domain must be transform to a discrete form, it means that signals must be sampled and quantized. The bandwidth of the controller developed in matlab was selected to be 100Hz. A reasonable rule of thumb for selecting the sampling frequency is that it must be between 10 and 20 times the systems close loop bandwidth [28]. It can be higher if the microcontroller is able to do it. The microcontroller was programmed to generate an ADC interrupt in such a way every T seconds the A/D converter sends the current and voltage value to the computer. The software used to interact between the microcontroller and the computer was the free software Code composer CCS provides from Texas instrument. The ADC operating clock speed has been selected to be 25MHz. To develop a current controller in a digital signal process (DSP), the differential equations must be transformed into a difference equations, and the signals are not continuous any more but discrete fig.3-12. In the analysis of continuois system we use the laplace transform, manwhile for

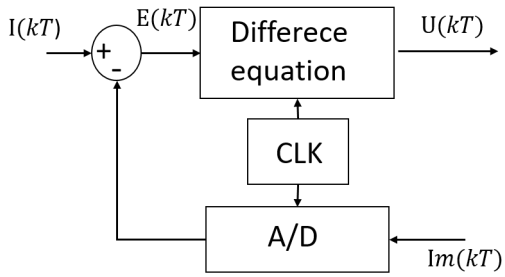


Figure 3-12: Digital control block.

discrete systems a similar procedure is available in the called z-transform [28]. From the Z-transform of a discrete system, the difference can be obtained by using the shift

properties (3.35)(3.36) [28].

$$Z(f(k+1)) = zF(z) \tag{3.35}$$

$$Z(f(k-1)) = z^{-1}F(z) \tag{3.36}$$

where f(k) is the sampled version of a continuous function f(t). There are two basic techniques for finding difference equations for a digital converter: discrete design adn discrete equivalent [28]. In this task, the discrete equivalent technique is used. It consists in designing the continuos compensator $C(s)$ and then get difference equation by Tustin method, ZOH or another method. For discretizing controller Tustin method is generally used because it does not create any delay compare to ZOH or first order hole FOH etc. The equivalent of the controller in z-transform is developed in (3.37) , where the transfer function operator s is replaced by $\frac{2}{T}\frac{z-1}{z+1}$.

$$\begin{aligned} k_p(1+T_i\frac{1}{s}) = k_p(1+T_i\frac{T}{2}\frac{z+1}{z-1}) \\ k_p(\frac{z-1+T_iT(z+1)}{2}) = \frac{u_z(z-1)}{e_z} \\ k_p(\frac{1-z^{-1}+T_iT(1+z^{-1})}{2}) = \frac{u_z(1-z^{-1})}{e_z} \\ e_z(k_p - k_pz^{-1} + T_i\frac{T}{2}k_p + T_i\frac{T}{2}k_pz^{-1}) = u_z - z^{-1}u_z \end{aligned} \tag{3.37}$$

or real time systems, negative subcripts in z are related to pass samples whereas positive subcripts are used for future samples. Hence, the difference equation is as follows (3.38).

$$u_k = k_pe_{k-1}(T_i\frac{T}{2} - 1) + e_kk_p(T_i\frac{T}{2} + 1) + u_{k-1} \tag{3.38}$$

This equation as been implemented in C-code, both the input and the output of the digital controller are vectors of two positions the first position for the past value and the second one for the actual value. Once the controller is implemented in c the output regulator leads the duty cycle for the PWM command. Firstly the output of the digital controller must be update and a function to limit the duty cycle between

0.01 and 0.99 is created for safety issues. The PWM is established as it is explained in [29]. The PWM used is the generic ePWM instance 1 where PWMA and PWMB are not working in complementary mode, it is because the driver L6392 inverts the signal. The setup PWM and ADC registers as well as the code for the control inside the ADC interrupt can be seen in appendix A. Notice that this code represents just the boost operation mode. In buck mode the the duty is calculated dividing the Vcommand into the Vbus.

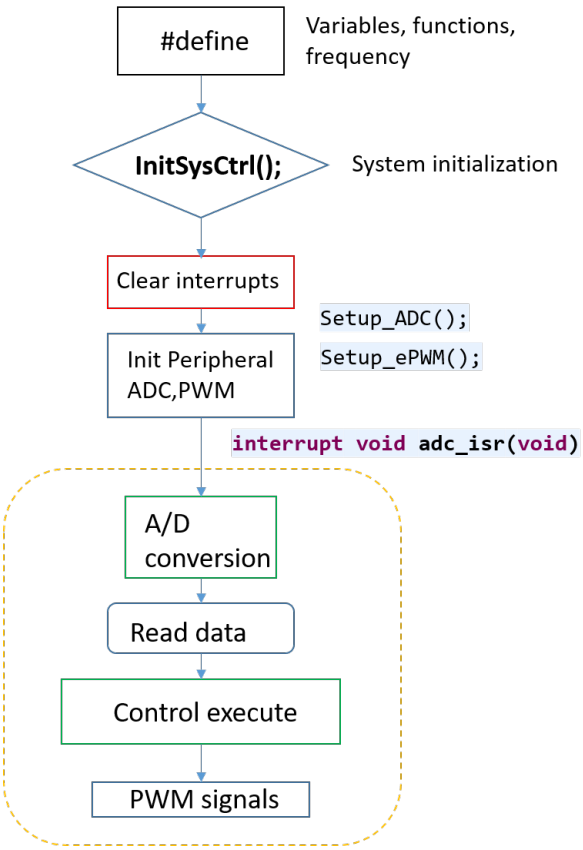


Figure 3-13: Flow chart of the current control in the DSP.

## 3.2 SOC

### 3.2.1 Overview

Once the converter has been built and tested in the lab the next step was to evaluate the lithium ferro phosphate (LiFePO4) cell. The first test was related the state of charge estimation. State of charge (SoC) of battery is the most important parameter to monitor and to maintain in the corresponding working range, so that the resulting shorter battery life due to its depth of discharge and battery overcharged risk can be avoided. The SoC of battery can not be measured directly but it could be estimated from measurement of several parameters such as voltage and electric current. The most common technique to estimate SoC is couloumb counting. This method consists in the straightfraward application of the equation.(3.39), it is an inexpensive method , reliable and easy to implement and widely used to get knowledge between open circuit voltage and capacity cell [4] [30]. A coulomb counting technique has many drawbacks such as error in integration process, difficult to estimate the initial $SOC(t_0)$ etc. Most of them has been explained in previous chapter.

$$Q(t) = Q(t_0) - \int_{t}^{t_0} i(t)dt \tag{3.39}$$

The aim is to get knowledge of charge and discharge profiles, controlling the current with the converter. The battery voltage and battery current is measured with an oscilloscope yokowaga DL850. The array provided by the oscilloscope is an structure with time. Therefore, and according to the coulomb counting equation (3.39), the capacity Q in Ah is obtained. According to the manufacturer the maximum voltage of the lithium cell (3.65V) would correspond to the maximum state of charge (100%) whereas a 2.4 voltage battery corresponds to a 10 % of SOC.

### 3.2.2 Experimental results

Fig.3-14 and 3-15 show the state of charge of a random LiFePO4 cell when charging and discharging process, respectively. It is charged at its maximum voltage for the

discharge profile and discharged to 2.0 V for the charge curve. From graphs, one can appreciate that the OCV vs SOC curve presents a very flat profile between 20% and 80% of state of charge,this phenomena in lithium ferro phosphate batteries is well-known and commented in literature [19] [30]. It implies a very accurate voltage measured, in the range of mV, to get a good approach, otherwise a small mismatch in OCV may cause a large deviation when used for SOC estimation. As the charge current increases, the profile is moved to bottom-left, the same occurs when discharge process fig.3-14 and fig.3-15.Based on the studies presented in [31] and [32], there are mainly three observable voltage plateaus and two transitions over the flat area on the OCV curve of LiFePO4 battery cells. It can be seen in the 0.12C discharge curve, or 25C curve. It provides the most information related to the open circuit voltage compares to state of charge cell because is done during 25 hours and as the current is very low the voltage cell almost remains constant. The lower voltage variation, the better relation between OCV and cell current [3].

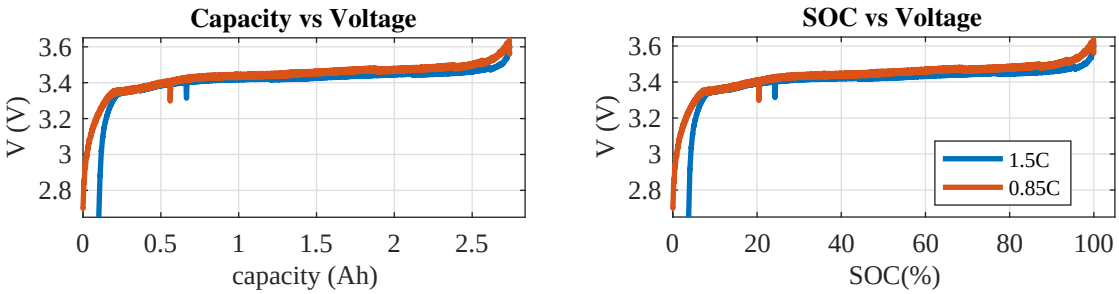


(a) Q(Ah) vs OCV. (b) SOC vs OCV.

Figure 3-14: SOC charge profile

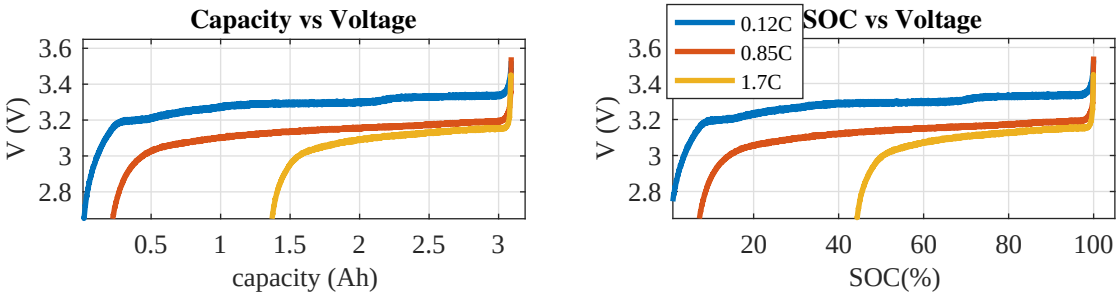


(a) Q(Ah) vs OCV. (b) SOC vs OCV.

Figure 3-15: SOC discharge profile

## 3.3 Internal impedance

### 3.3.1 Overview

Batteries are not an stationary element. In a passive element like resistances the ability to opposite the current flow when a differential voltage is applied can be obtained be the ohms law. However, it implies several simplifying properties as the resistance is independent of the frequency, the AC current and voltage signals through a resistor are in phase with each other. These kind of assumptions cannot be adopted when working with batteries, as they are an active element whose internal impedance varies depending on the operation point. Basics of EIS, have been more deeply explained in the state of the art section. To measure the electrochemical internal impedance ($Z_{bat}$) a singular and expensive equipment is needed. Z is usually measured by applying an AC potential to a cell and then measuring the current through the cell. Assume that we apply a sinusoidal potential excitation. The response to this potential is an AC current signal.

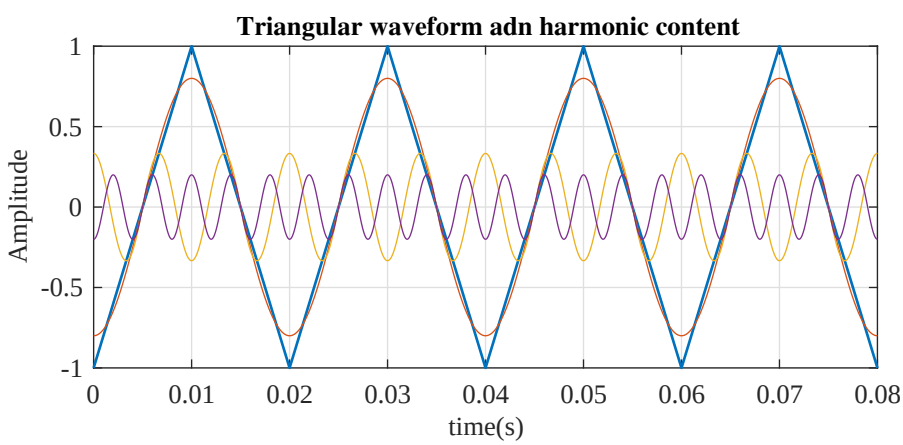


Figure 3-16: Harmonic content in a triangular waveform.

The equipment allows static impedance measurement, it means that the battery must be in repose. However, the idea of AC signals for measuring impedance are extrapolated in the case when the battery is working. The DC DC bidirectional converter allows to test the cell, in both cases discharge and charge at different rates of

C. The inductor current or battery current measured is a triangular waveform. The DC current defines the overall working point of the battery and the AC signal can be analysed as a sum of sinusoidal functions, sin and cos, by means of Fourier series. Physically speaking these mathematical functions are the harmonic content in the real battery current signal fig.3-16.

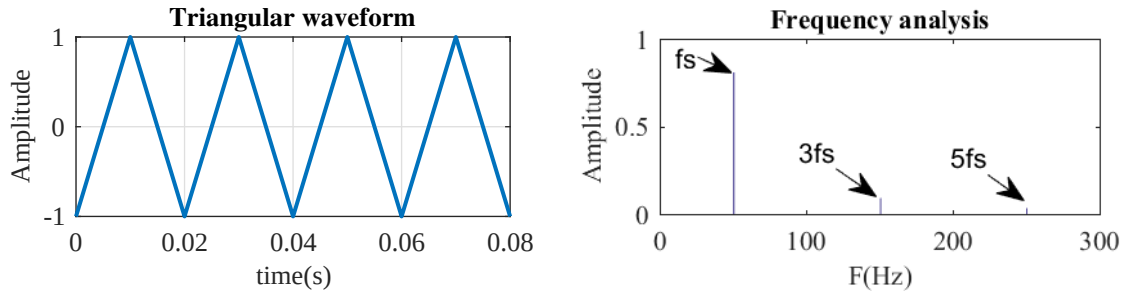


(a) Triangular waveform (b) Triangular waveform frequency analysis

Figure 3-17: Ideal triangular waveform

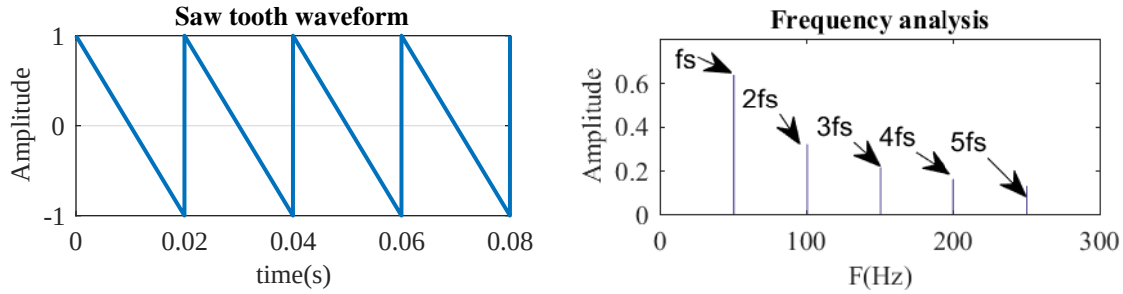


(a) Saw of tooth waveform (b) Saw of tooth waveform frequency analysis

Figure 3-18: Ideal saw waveform

Current and voltage are measured considering the passive sign convention. It means that when the battery is discharging the current obtained with the oscilloscope is multiplying by -1. However, this implies assuming the battery as a passive element which cannot be correct. The switching frequency produces charge and discharge inductor at that frequency thus the triangular waveform measured will be at 15kHz. The harmonic content in voltage and battery current due to the switching frequency, are AC signals whose amplitude differs form the fundamental frequency according to the Fourier coefficients [33]. An ideal triangular, periodic signal defined in an interval

would produce odd harmonic content, it means($3f_s$,$5f_s$) fig.3-17, whereas a saw of tooth wave has all of the harmonic content fig.3-18. These frequency analysis should be take into account when processing the real signals because the current through the inductor are not a pure periodic triangular wave where only odds harmonic appears. To sum up, these AC signals are using to get the impedance battery at different frequency and at different working points superimposed by the DC current controlled.

### 3.3.2 Experimental data and results

Fig.3-19 and 3-20 shows real signals captured with a Yokowaga oscilloscope. The data are processed off-line using matlab(Appendix A). As it can be seen the real signal contents all of the harmonics integers multiples of the switching frequency ($f_{sw}, 2f_{sw}, 3f_{sw}, f_{sw}, etc.$), this is because it is not neither a pure periodical signal nor a pure triangular signal defined in an interval [33]. Therefore, the interior impedance battery will be given at $nf_{sw}$ (3.40) being the switching frequency 15kHz.

$$Z_{nf} = \frac{V_{nf}}{I_{nf}} \tag{3.40}$$

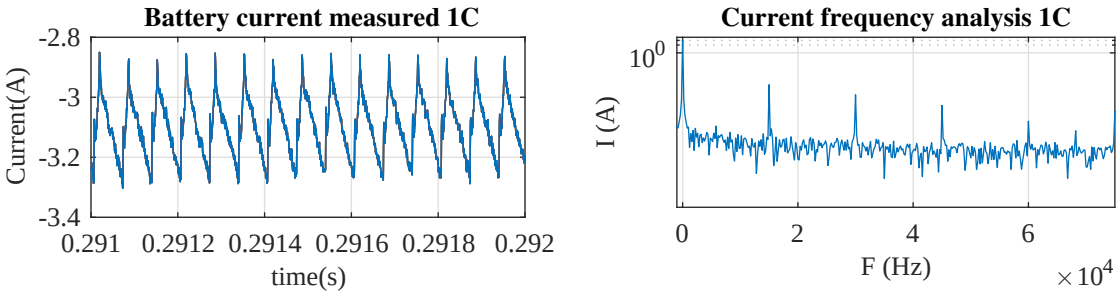


(a) Battery current time domain (b) Battery current frequency domain

Figure 3-19: Battery current 1C

Fig.3-21 shows the interior DC resistance from different SOC during discharge process. The X-axis represents current and Y-axis the cell dc resitance in ohms, calculated from equation.3.41. The battery have been discharge from 0.25C to 2C rates of current. As we can see the higher the cell state of charge, the lower the

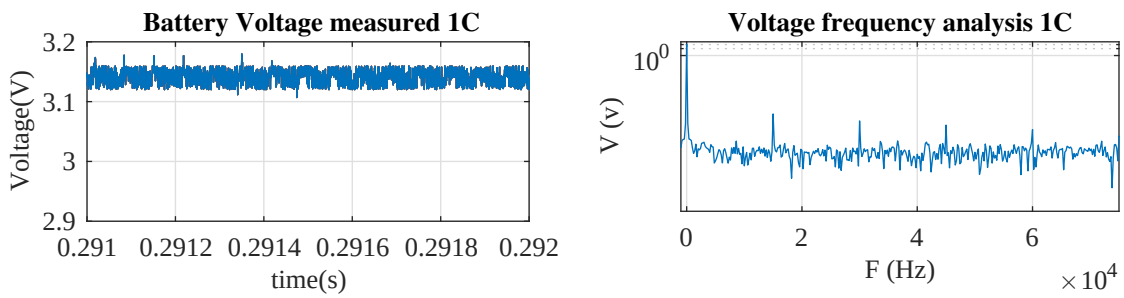


(a) Battery voltage time domain (b) Battery voltage frequency domain

Figure 3-20: Battery Voltage 1C

resistance, and it decreases as the current increases.

$$R_{dc} = \frac{(V_0 - V_{dc})}{I_{dc}} \tag{3.41}$$

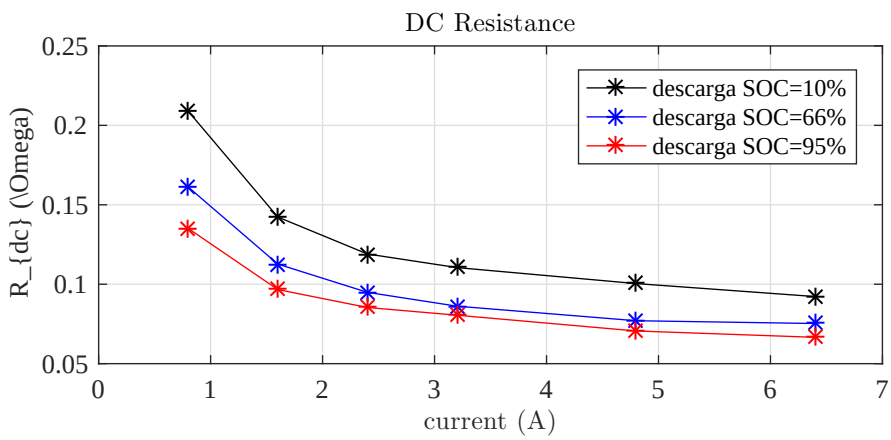


Figure 3-21: LiFePO4 DC resistance.

The DC resistance is an important parameter to take into account but it does not affect the design of the rest of the system devices. However modelling the dynamical behaviour of electrochemical power sources at high frequencies when battery is working is an important issue for designing controllers, filters and other system elements sensitive to produce resonance. Therefore the aim of this research master thesis is to get knowledge about the behaviour of the cell when working at 15kHz

which is the switching frequency. These behaviour is evaluated through the internal impedance battery. As it was explained before the switching harmonics allows as to get the impedance at integer multiples of the switching frequency. As it can be seen in the script appendix A, it is important to adapt the number of samples in order to avoid harmonic dispersion, which could lead errors. Results are presented as follows: three battery cells, at different SOC levels, have been tested. The current rate is controlled in both charge and discharge process from 0.25C to 2C, it means 0.8A and 6.4A. Therefore, we have eight different impedance value, one for each current rate. The black, blue and red curve represent 10%, 66% and 95% SOC, respectively. Fig.3-22 , fig.3-23 and fig.3-24 show the cell impedance at 15kHz, 30kHz and 45kHz, respectively during the discharge process. Left graphs represent the resistance part whereas those figures to the right part. Impedance behaviour is shown until the 3th harmonic because, harmonics at 60kHz, 75kHz and so on, present a very low magnitude in the amplitude that could lead errors when calculating the impedance. On the other hand, the impedance battery is not so relevant above 45kHz because according to the circuit elements resonance takes place at lower frequencies.

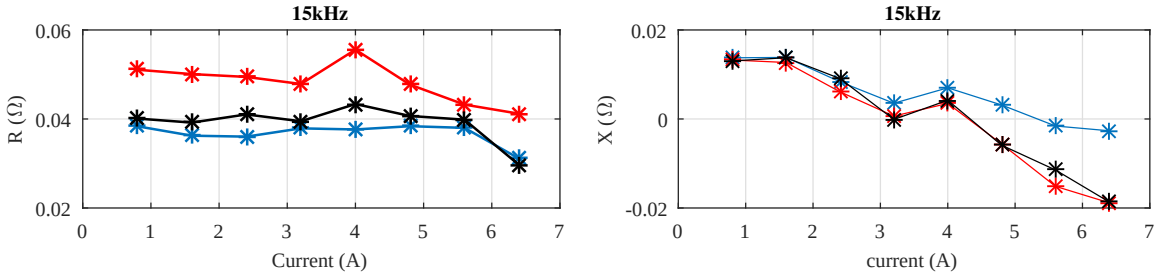


(a) Real part

(b) Imaginary part

Figure 3-22: Cell impedance at 15kHz discharge process.

AS it can be seen, cell resistance $R(\Omega)$ increases as the frequency increases, it is basically due to the current amplitude decreases with frequency. Moving on to the reactance part, experiments shows a change in the reactance behaviour at high currents. In particular when the current is above 1C (3.2A) the cell changes from the inductive behaviour to the capacitive behaviour during a discharge process and viceversa when charging. Literature [10] [11] [8] explains that the vast majority of lithium

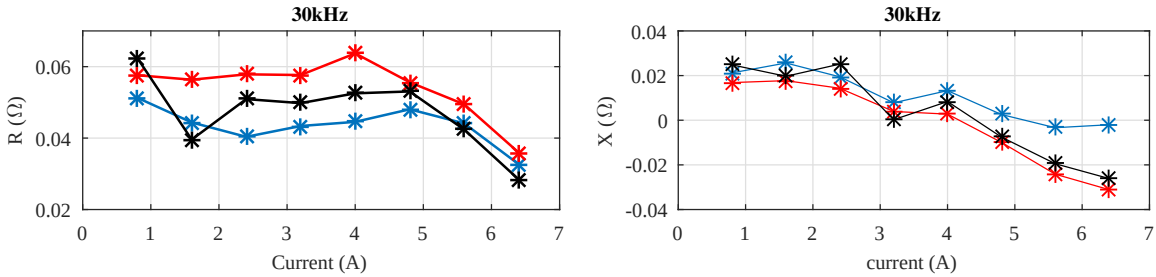


(a) Real part (b) Imaginary part

Figure 3-23: Cell impedance at 30kHz discharge process.

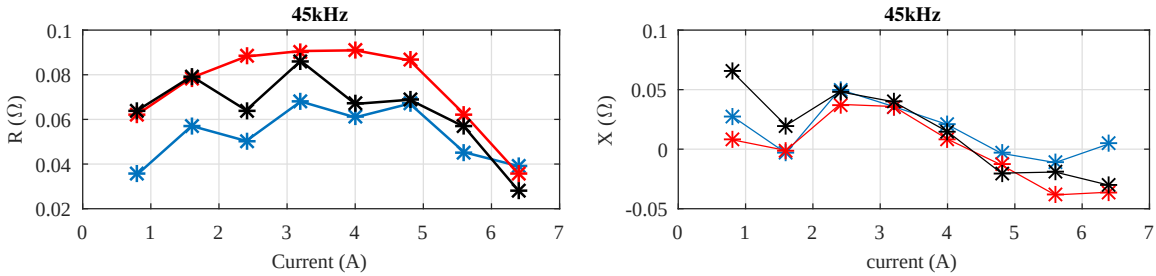


(a) Real part (b) Imaginary part

Figure 3-24: Cell impedance at 45kHz discharge process.

batteries, especially lithium ferro phosphate cell, shows an inductive behaviour at high frequency, normally above (1kHz) [8]. This statement is justify looking at experiment results however no information is related to high frequency, where reactance behaviour changes. The LiFePO4 tested cells in the present thesis, are new cells and high quality fabrication. According to the manufacturer the recommendation current rate in both charge and discharge is 1C. This could be highly related to the behaviour cells, but it cannot be explained. Further work could study other chemistry cells, lower quality liFePO4 fabrication cells even the same cell after many cycles of life. The results expected should be a change in the reactance behaviour even before than 1C or a higher resistance part.

The same results are shown in fig.3-25,3-26, 3-27, but now during the charge process the behaviour changes from capacitive to inductive. Similarly than before there is an increment in resistance cell as frequency rises. Notice that there is not almost dispersion between cells at different SOC.

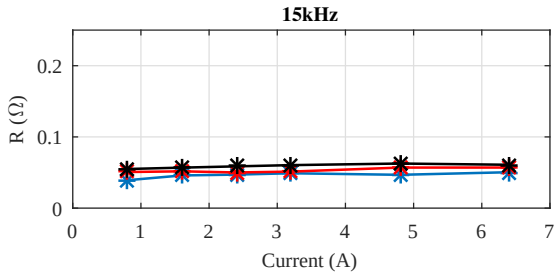


(a) Real part

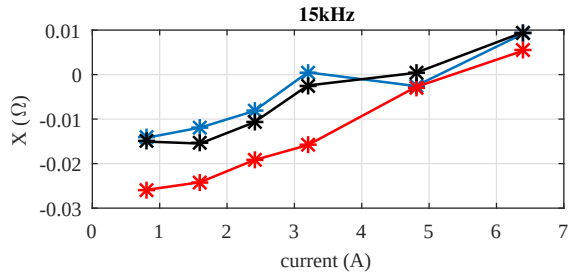


(b) Imaginary part

Figure 3-25: Cell impedance at 15kHz charge process.

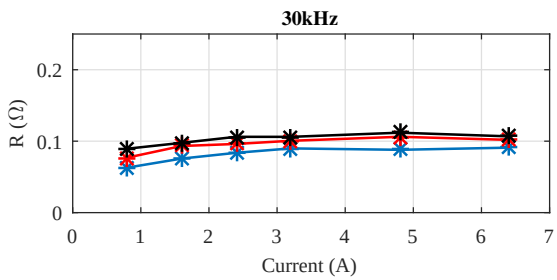


(a) Real part

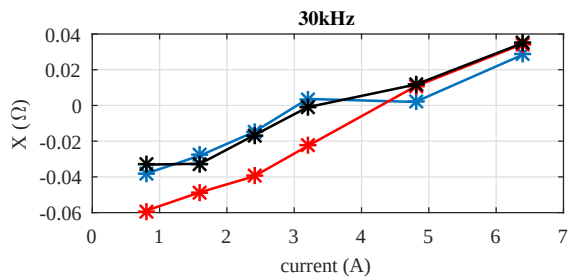


(b) Imaginary part

Figure 3-26: Cell impedance at 30kHz charge process.

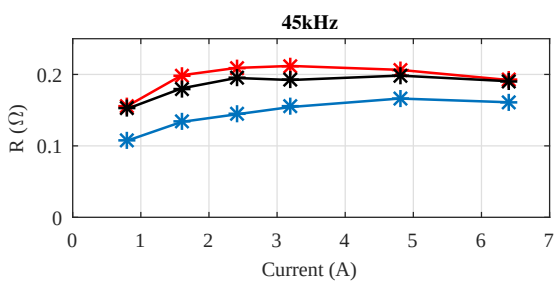


(a) Real part

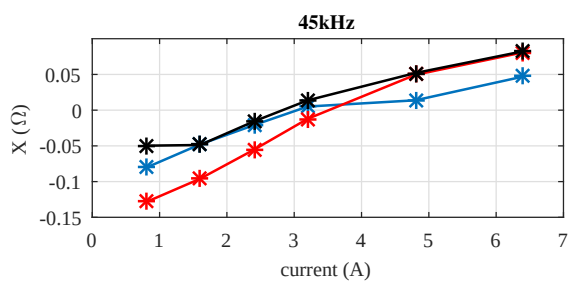


(b) Imaginary part

Figure 3-27: Cell impedance at 45kHz charge process.

# Chapter 4

# Static battery Model

The behaviour of electrochemical units was subject to several modelling suggestion as explained in [10],[8],[11]. As it was mentioned in the state of the art section, a electrochemical cells could be represented by partial differential equations, that results in heavy computational mathematical process. Instead, electrical models are used. However, parameters for developing these electrical models are obtained when the battery is resting, therefore it is an static model. Since battery are non stationary, in this chapter an electrical model of a LiFePO4 battery cell is obtained. Then this static parameters are compared to those obtained in the previous chapter, when the battery are working.

## 4.1 Randal electric model

The most popular battery electric model is the randal model 2-1 [8] [9], and there are different ways to get the electric parameters.

The method uses in the present master thesis to perform a model, is the electrochemical impedance spectroscopy. EIS compared to step response methods allows for a direct measurement in any working point [10] [11]. Moreover, to compare cell static impedance and dynamic impedance, the EIS provides a unique tool , because harmonics small signal excitations can be done in wide frequency range from low

frequencies(mHz)to high frequencies (kHz). The issue here is that laboratory instrumentation , need for high precision impedance measurement, EIS meter, is an expensive materil tat is not available in the lab. The strategy to perform small AC current signals, which allow us to carried out the EIS method is to use a generator frequency. By adjusting the offset of the generator frequency with the cell voltage, ensure that there is not current flowing between the cell and the generator. During an impedance measurement , a small AC current generated with the voltage amplitude of the frequency generator flows through the cell under investigation and the AC voltage response is measured. The current is obtained by measuring the voltage drop in a shunt precision resistor (0.1Ω). The circuit topology can be seen in fig.4-1. Data

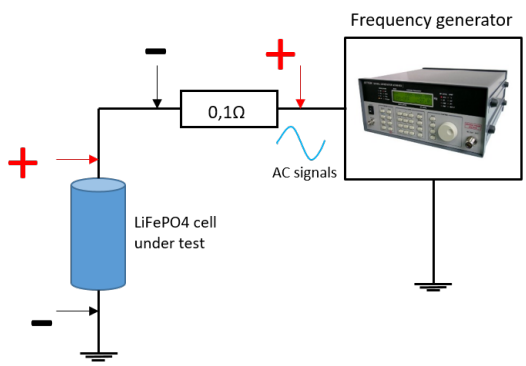


Figure 4-1: EIS meter.

are collected with yokowaga oscilloscope and afterwards they are processed in matlab as it was done before (Appendix A). The analysis is done in frequency domain and the representation of the battery impedance is plotted in a nyquist diagram where y axis represent the reactance and x-axis the resitance. Fig.4-2 shows the internal impedance of a LiFePO4 cell charged at its 70% of capacity. The AC signals injected in the battery goes from 100mHz to a 50kHZ, however in this figure it is just shown the capacitive impedance. Above 500Hz the battery reactance behaviour changes to inductive. Notice that the y-axis are negative values. In literature [10],[11],[8],[9] static model parameter are obtained by the capacitive behaviour of the cell. As stated

in chapter one, a commonly electrical model is the called randal cell fig.4-4 [8]. In this chapter an static model of a LiFePO4 has been developed, an electrical model and obtaining the parameters from the EIS method. The parametrization is as follows.

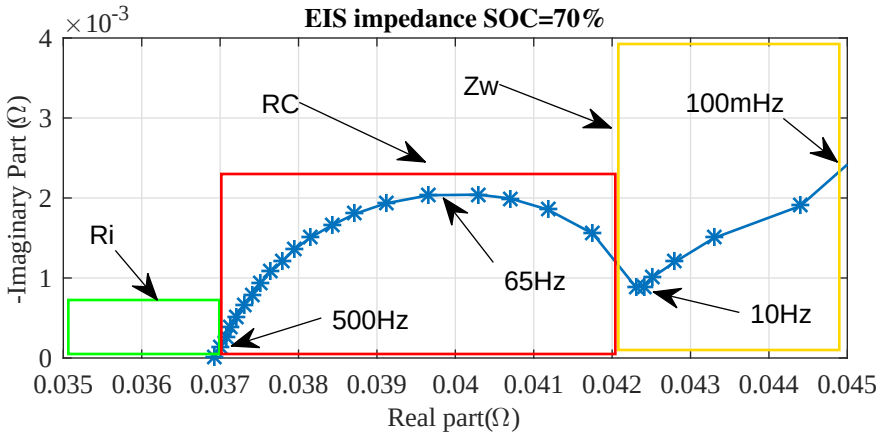


Figure 4-2: Electrical impedance spectrum of a LiFePO4 cell at 70% of SOC.

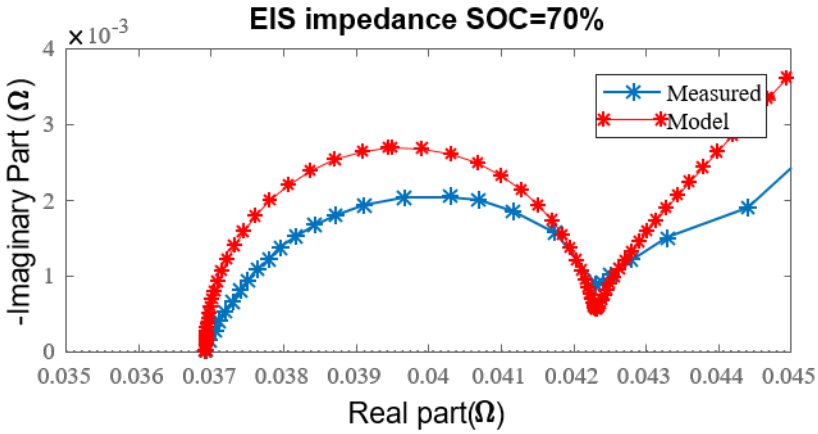


Figure 4-3: Electrical impedance spectrum of a LiFePO4 cell at 70% of SOC and electrical cell model.

Every battery shows an ohmic resistance $R_i$ which is due to the limited conductance of the contacts [10]. The value are represented in the green rectangle fig.4-2, it represents when the battery behaviour changes from capacitive to inductive. The transient response of the battery electrodes is characterized by the semicircle insisde the red rectangle, where $R_c$ is the approximately the radius of the semicircle and C is ex-

tracted form the tau constant $\tau = RC$ represented by the maximum impedance point (top of the semicircle). THe most challenging component to identify is the Warburg impedance $Z_w$ as it depends on the electrons diffusion and concentration. Several methods have been proposed to model the diffusion phenomenon. In our study a series of RC circuit are used to represent $Z_w$ fig.4-4(b) [8]. A maximum number of five RC circuit is limited [10].

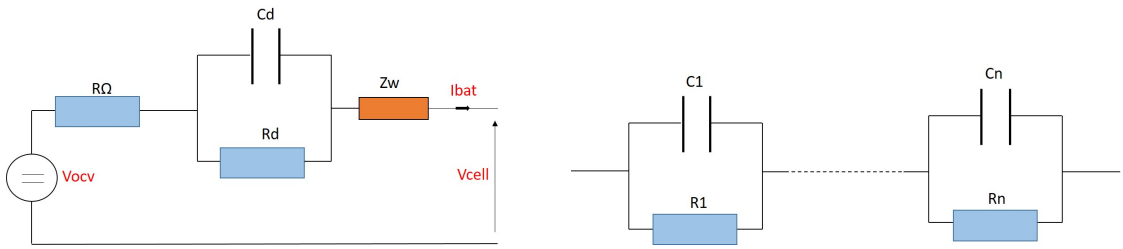


(a) Randal electric model cell (b) Series of RC circuit

Figure 4-4: Basic electric model.

Table 4.1: Parameters randal model

| **Parameter** | **Value** |
|---|---|
| Ri | 0.0369Ω |
| Cd | 1.55F |
| Rd | 0.0054Ω |
| R1 | 0.0203 |
| C1 | 2834F |
| R2 | 0.0023Ω |
| C2 | 2834F |
| R3 | 0.0008Ω |
| C3 | 2834F |
| R4 | 0.0004Ω |
| C4 | 2834F |
| R5 | 0.0003Ω |
| C5 | 2834F |

The total electrical model impedance is given by equation(4.1) Taking into account the assumption of a series RC circuit the mathematical expression of the Warburg impedance is depicted in(4.2). where s is the Laplace operator and $R_n$ and $C_n$ are expressed in relation with kq and k2 as it can be ssen in eq.(4.3) (4.4) [8].

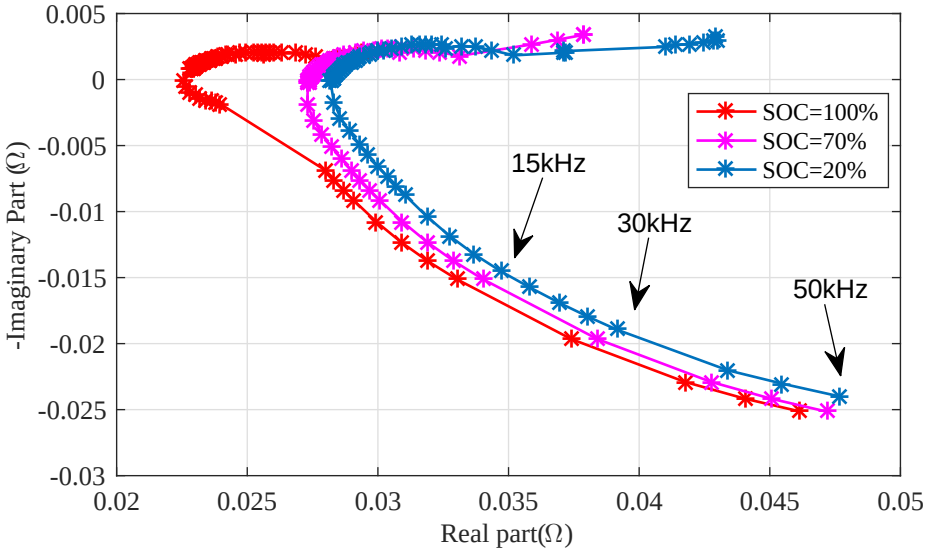


Figure 4-5: Electrical impedance spectrum of a LiFePO4 cell at different SOC

$$Z = R_i + \frac{R_d}{1 + R_d C_d s} + Z_w \tag{4.1}$$

$$Z_w = \sum_{i=1}^{n} \frac{R_i}{1 + R_i C_i s} \tag{4.2}$$

$$R_n = \frac{8k_1}{(2n-1)^2 \pi^2} \tag{4.3}$$

$$C_n = k2 \tag{4.4}$$

Table.4.1 summarize the parameters obtained y the electrical impedance spectrum of a LiFePO4 cell at 70% of SOC. Fig.4-3 shows the static electrical cell model and the electrical impedance spectrum for a Lithium ferro phosphate cell (70%) of SOC. The battery model developed is an static model very used in literature related to battery models. It will depends on many parameters such as temperature that highly affects chemical cell, state of charge, number of cycles and ageing cells [6]. The changes in electrical impedance spectrum due to temperature or ageing cell can not be demonstrated in this thesis. However, the deviation in the internal impedance of a cell with different states of charges can be seen in fig.4-5. As the SOC increases,

spectrum curves moveto the left. It means that The higher SOC the lower resistance ohmic resistance.

## 4.2 Static model vs dynamic model

Altough Static models are well-established and deeply studied , most of them are focused on low impedance battery and warbourg impedance studied as in [10], [20], [9], [11].

However for our case of studied high frequency impedance is more important in order to avoid resonance and to get knowledge about the plant model system in order to help control design for current and voltage regulator in converters. On top of that Since, the battery are not stationary elements and non-linear the dynamic behaviour are much more important for our study than the static behaviour. Fig4-5 shows the impedance spectrum of three LiFePO4 cells with different state of charges. As it is established in literature the reactance cell tends to be inductive. These cells are resting, it means off-line, so one of the aim of this master thesis is to demonstrate how the impedance varies when they are working.

Fig.4-6 shows the the difference when the battery is in repose or when they are in the discharge process. The impedance value of the discharge process are those obtained in the previous chapter using switching harmonics. Therefore, just those impedance available by the converter are compared, it means at 15kHz, 30kHz, and 45kHz, but from the picture one can appreciate that the curve follows a tendency. The initial state of charge cell is 70% and firstly the EIS experiment have been carried out in order to avoid that these state of charge resulted modified. Afterwards the same cell was tested in a the bidirectional converter, discharging the current at 0.5C, 0.75C and 1C.

For instance experimental results deliver that the variation in the internal impedance battery can achieve almost a 28% at 15kHz and a 15%at 30kHz. Nevertheless these

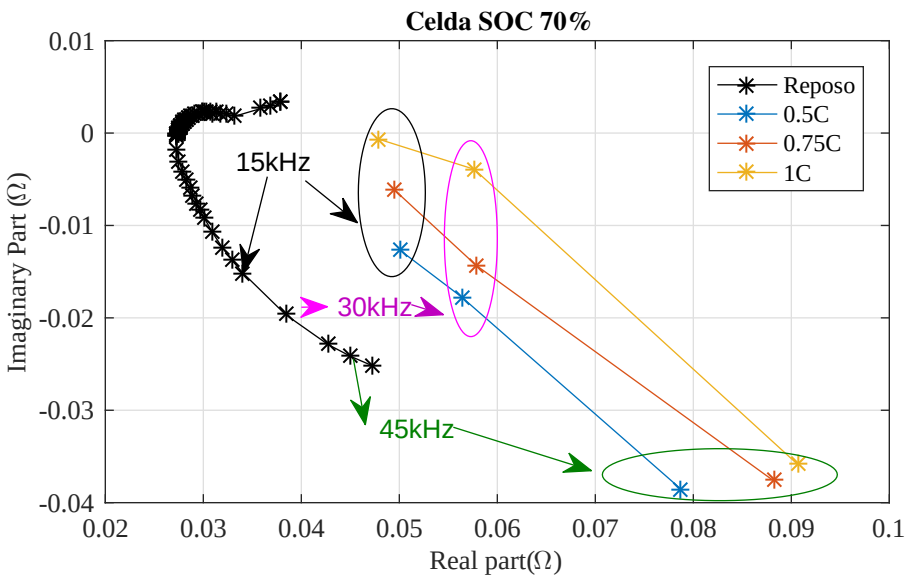


Figure 4-6: Dynamic and static electrical impedance spectrum of a LiFePO4 cell at different SOC.

numbers are just applicable to an specific case of 70% of state of charge, at 25°$C$ of temperature and for a LiFePO4 chemistry. Obviously, different SOC, temperature and agieng cells would deliver difference results. Another interesting thing, is that the current rate increases, the impedance spectrum curve seems to move up to the capacitive part. This phenomena has been also seen in the previous chapter when currents above 1C (3.2 A) altered the impedance cell behaviour from inductive to capacitive.

# Chapter 5

# Cell balancing

As stated in the state of the art, a BMS protects battery system from damage, predicts and increases battery life and maintains the battery system in an accurate and reliable operating condition. One of the main problem of battery strings made by cells is the imbalance making a major threat to the system battery life. Without the balancing system, the individual cell voltages will drift apart over time. As well as, the usable capacity of the total battery pack will also decrease more quickly during operation that leads to fail the whole battery system [4].The battery balancing topologies can be divided into passive and active balancing. The former one removes the excess energy from the fully charged cell(s) through a passive element, the resistor, until the charges match those of the lower cell(s) in the pack or a charge reference level.The active cell balancing methods remove the charges from higher energy cell(s) and deliver it to lower energy cell(s). Although, passive methods are widely used due to its costless adn simplicity, it seems to be clear that the challenge for the future is to develop active balancing methods which improves the efficiency of the system. Active cell balancing methods have been reviewed in the state of the art of the present thesis and obviously the decision to use one method or another strongly depends on the application.

The whole battery pack used in this project consists on 16 modules, with 255 cells placed in a matrix of 15x15. Apart from dynamic models and impedance battery

behaviour this master thesis deals with an equalization cells inside each module. Due to the higher number of cells to balance inside a pack , the use of converter makes the application either very complex and expensive. Passive methods, where extra energy are dissipated in resistance could be an option however voltage sensor are needed to command the switches which makes the application expensive. It goes without saying that the system efficiency might be quite low. On top of that the dissipative heat inside a pack could lead thermal problems. Based on this requirements, the equalization cell method chosen is the swithced capacitor balance cell. The first referenced for this method is in [24], however there are no references where the method had been implemented. In this project a switched capacitor prototype have been implemented in the lab for balancing four LiFePO cells.

## 5.1 Switched capacitor equalization cell

The switched capacitor (SC) is illustrated in fig.5-1. The basic requirements are n-1 equalized capacitor and 2n switches for balancing n number of cells. One of the characteristics of the topolgy is that the control strategy is very simple because it has only two states, shuttling between the whole cells sequentially, moving the switches frequently from the upper position to the lower position and again to the upper one with a small rest period between each transition and so on. In addition, it des not need any control strategy, it can work in both charging and discharging mode and according to literature [24],[15] it has a reasonable efficiency although it is not easy to measure. These previous reasons help to made the decision to use this kind of topology in the project thinking that the system could be scalable to balance 255 cells.

### 5.1.1 Basics of operation

The operation of the topology is very simple. As it was explained before there is no any control and both switches upper and bottom will work with the same duty cycle. In such acase the capacitor will charge at the voltage cell in a half of period $\frac{T}{2}$

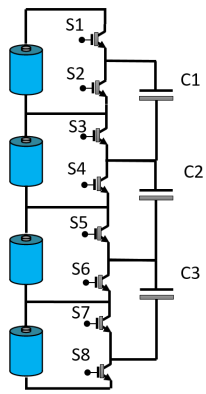


Figure 5-1: Switched capacitor cell balancing topology.

afterwards the discharge will take the same amount of time $\frac{T}{2}$. Fig.5-2 shows the case when upper switches are on. Notice that the same signal is for all of upper switches at the same time. In this operation state $C_1$ is paralleled with $cell_1$ and therefore $C_1$ is charged or discharged depending on if its voltage is greater or lower than the cell voltage, in any case the capacitor voltage will obtain the same voltage than the cell. Fig.5-2(b), we can see an example where $C_1$ is charged from its previous state

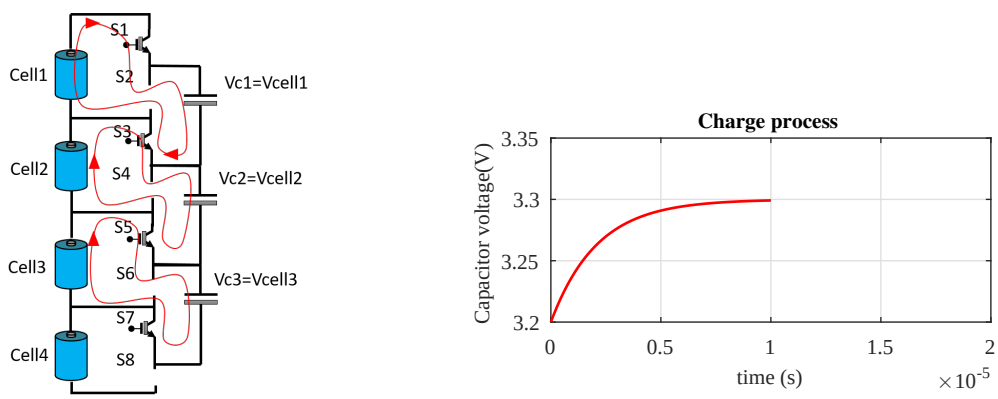


(a) Upper switches on

(b) Capacitor charge

Figure 5-2: Switched capacitor topology, upper switches on.

of 3.2 V lower voltage cell ($V_{cell2}$) to the upper voltage cell 3.3V. Then after this process the system will turn to the other state shown in fig.5-3. In this state ll of the bottom switches are on whereas the upper ones are off. Analysed the same capacitor than before $C_1$, it will be now paralleled to $cell_2$, as $V_{cel2}$ is lower than $V_c$ the capacitor voltage is discharged fig.5-3(b). The same thing will happen in this state as

the previous state and after cycles the proposed circuit is intended to equalize cells. To achieve and to check the circuit behaviour a simulation has been carried out in

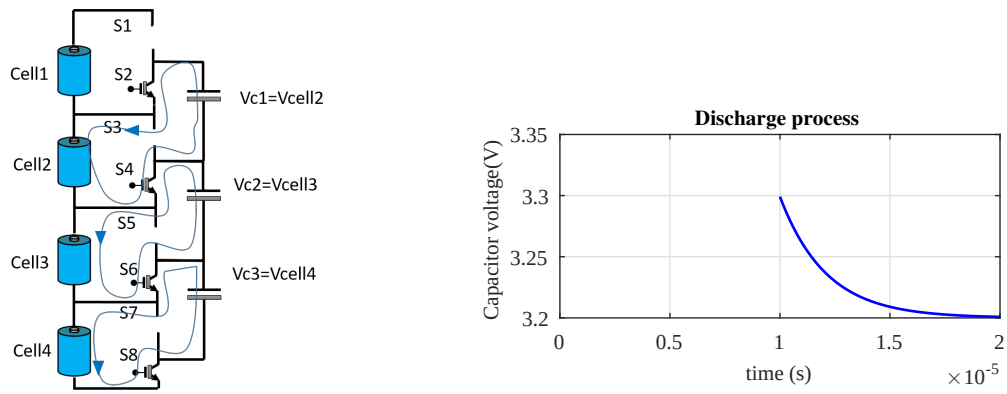


(a) Bottom switches on (b) Capacitor discharge

Figure 5-3: Switched capacitor topology, bottom switches on.

psim software , A capacitor value is $22\mu F$, with a series resistance that represents the equivalent series resistance capacitor (ESR) plus the on mosfet resistance $R_{on}$. The frequency is 50kHz, and the duty cycle 0.5. Fig.5-4 shows that after a time the voltage cell have been equalized, using this topology. Of course the time is adjusted for the simulation because as it was explained before the switched capacitor topology is takes a long time to balance cells. The time of equalization is related to the

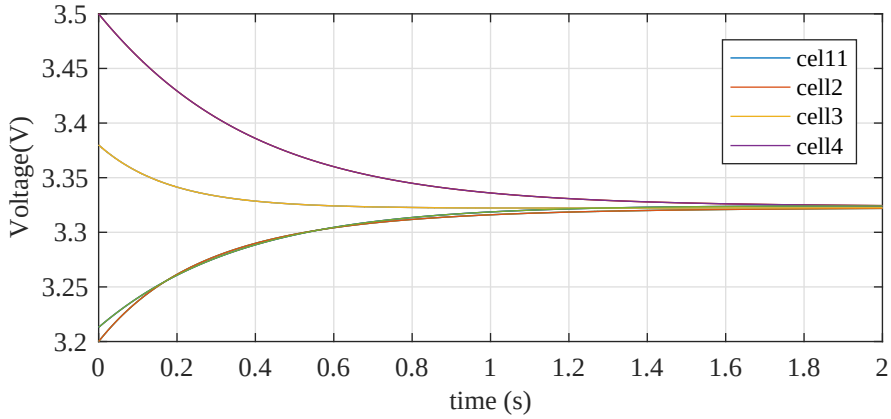


Figure 5-4: Equalization voltage cell psim simulation.

the capacitor capacity, the resistance of the components such as ESR, $R_{on}$ mosfets, internal battery resistance, wires etc. The higher the unbalance between two cells, the

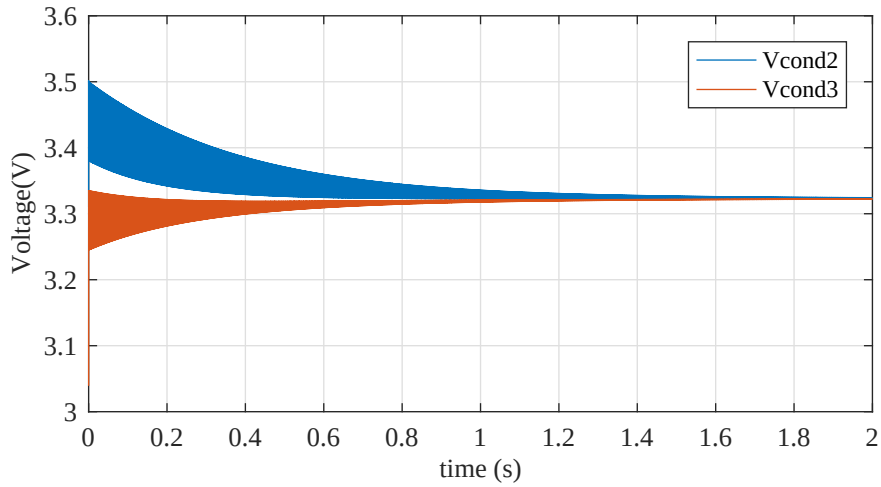


Figure 5-5: Voltage capacitor psim simulation.

faster the equalization between them, this is because there will be higher differential voltage then more current flowing. The energy moved between cells depends on the equalization capacitor and the voltage (5.1), so higher capacitors are able to move more energy, however selecting an oversized capacitor might cause that it does not charge itself completely that produce a capacitance waste. So it seems to be clear that there will be an optimum capacitor that makes the circuit topology more efficiency. In our case of study the capacitor selected have been based on the lowest ESR available in the lab, and the switching frequency have been adjusted to its value in order to get completely cycles of charge and discharge. Obviously, in LiFePO4 chemical cells , where there is a very flat zone between 20% and 80% of SOC, the differential voltage between cells are so low that the capacitor is not charged completely.

$$E_c = \frac{1}{2}CV^2 \tag{5.1}$$

## 5.2 Lab implementation

The PCB switched capacitor design have been done with Altium software, as it was done fro the bidirectional DC DC converter. The components selected for the PCB have been selected according to power, current and votlage limits but an important

criteria has been to chose components with low resistance. As it was explained above the main reason is that the higher the impedance the lower the time to balance.

Table 5.1: Balancing switched capacitor components

| **component** | **Manufacturer** |
|---|---|
| Mosfets | NXP N-channel LFPAK 80 V 45 mΩ standard level MOSFET |
| $C_{eq}$ | Condensador de tántalo 22uF ESR=0.1 |
| Isolated DC DC | MEV Isolated 1W Single & Dual Output DC/DC Converters |
| Driver | L6392 ST |
| Opto | ACPL-m 46 T |

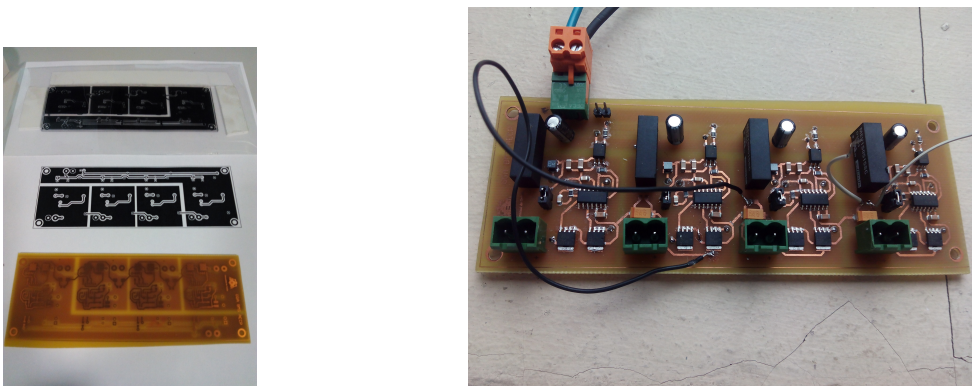

(a) PCB in process (b) Switched capacitor PCB

Figure 5-6: Switched capacitor PCB process

The capacitor is a $22\mu F$ tantalum capacitor with a ESR equal to 0.1Ω, the frequency have been selected to be 50kHz, increasing the frequency the ESR capacitance is low however the capacitor could be oversized for this frequency and it cannot be fully charged. The mosfet are N-channel mosfet with a $R_{on} = 45\Omega$.As shown above, each cell has installed two switches. To put the reference of the mosfet source to ground, isolated ground are needed. Fig.5-6, shows clearly the isolated ground planes. Due to this, isolated DC DC converters (5V to 5V) are used to supply the electronic components such as the driver and opto-couplers. the last one are needed to isolated the ground plane of every driver and the common ground plane. The signals are generated with a F28335 microcontroller form texas instrument, the program generates one square waveform with a fixed duty cycle of 0.5, and a switching frequency of 50kHz. the delay between signals are done by hardware with a recommended instal-

lation according to the datasheet of the driver manufacturer. Table.5.2 summarize the electronic components for the PCB prototype.

## 5.3 Experimental data and efficiency

To carried out a experimental balanced in the lab, four cells with different initial SOC, it means, different voltage have been established.

- $V_{cell1}$=3.242V ; SOC=23%
- $V_{cell2}$=3.307V ; SOC=73%
- $V_{cell3}$=3.419V ; SOC=99%
- $V_{cell4}$=3.171V ; SOC=8%

Previously, it was ,mentioned that greater differnrce in voltage between cells implies higher current, higher energy exchanged, then faster balance. The postion of the cells have been as it can be seen in figure 5-8(a). Moreover, according to code colors $V_{cell1}$, $V_{cell2}$, $V_{cell3}$ and $V_{cell4}$ are blue, red, magenta and gree, respectively. Fig.5-7 shows the experimental result of a four LiFePO4 battery cells. As it can be appreciate from the figure cells are finally balanced between them. The topology switched capacitor is demonstrated to be a low balance systems, as thee equalization cells took almost 48 hours. However, it has a huge number of advantages. The difference in voltage between them can be seen in fig.5-8(b), practically mV. Entering with these voltage values into the 25C state of charge curve fig.2.3. the difference in SOC are shown below:

- $V_{cell1}$=3.297V ; SOC=70.2%
- $V_{cell2}$=3.297V ; SOC=70.2%
- $V_{cell3}$=3.302V ; SOC=70.7%
- $V_{cell4}$=3.300V ; SOC=70.1%

Notice that the green curve that represents the lowest initial voltage cell after equalization overcomes the voltage cell one and voltage cell two. To sum up this is

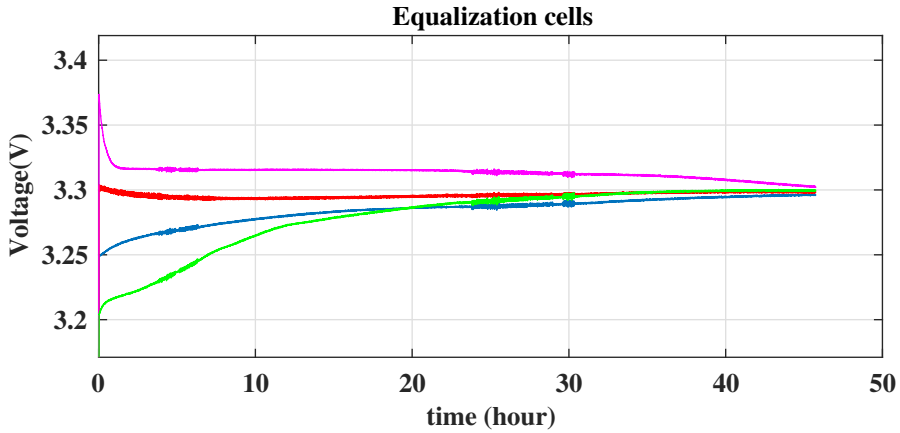


Figure 5-7: Voltage cells experimental results.

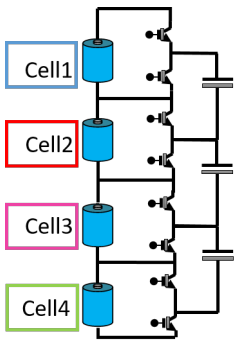


(a) Cell balancing topology

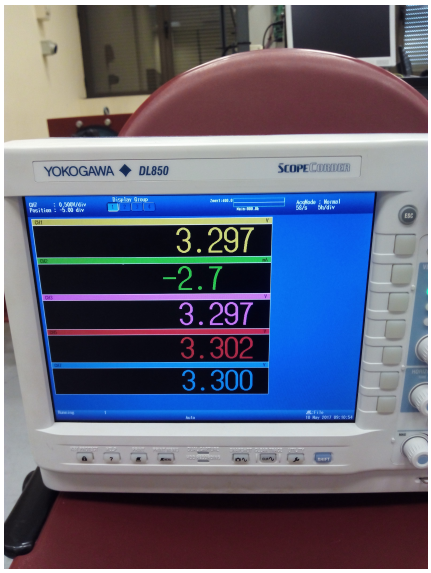


(b) Voltage cells after 45h of equalization.

Figure 5-8: Equalization cell prototype results.

equalization cell have been demonstrated to be a cheaper active balancing and simple to implement, and a good solution for hughe number of equalization cells shich is the case of the present project. The challenge here is to evaluate the efficiency of the converter, further works can be addressed to calculate the efficiency based on experimental results. In this work a theory approximation have been done.

### 5.3.1 Efficiency

The capacitor balance will transfer energy between lower voltage cell and higher voltage cell, the efficiency here is related to the energy transferred from the highest voltage cell to the capacitor and then the discharge energy to the lower voltage cell. So it is calculated in two steps. The energy is calculated during one charging period only, so that time will be from zero to one duty cycle. equation.(5.2) gives the energy transferred from the higher charge cell to the capacitor during the period DT in Ws/pulse. this energy is a function of the capacitor value, switching frequency, cells differential voltage , duty cycle and equivalent resistance that includes Ron mosfets, ESR and internal cell resistance extracted from the EIS impedance figure of a cell at 50kHz. Hence, the equivalent resistance is:

- Ron=0.045x2Ω
- ESR=0.1Ω
- $R_{cell}$=0.0475x2Ω

$$E_{charge} = \int_{Dt}^{0} V_c i_c dt = \int_{Dt}^{0} [V_{diff}(1 - e^{\frac{-t}{\tau}}) + V_i][\frac{V_{diff}}{R_{eq}} e^{\frac{-t}{\tau}}]dt = \int_{Dt}^{0} [\frac{V_{diff}^2}{R_{eq}} e^{\frac{-t}{\tau}} - \frac{V_{diff}^2}{R_{eq}} e^{\frac{-2t}{\tau}} \frac{V_i V_{diff}}{R_{eq}} e^{\frac{-t}{\tau}}]dt \quad (5.2)$$

Hence the integral is calculated in a half of period, with a duty cycle of 0.5, where Vi is the initial voltage of the capacitor and Vf the final voltage, it means the votlage between adjacent cells where the capacitor is connected. The energy is done in the form of Ws/pulse and multiplying by the switching frequency Fsw=50kHz, it is done in Wh/h, [34]. The capacitor transferred energy during one discharge pulse can be calculated from the capacitor discharge voltage and current as given in, 5.3

$$E_{discharge} = \int_{Dt}^{0} (\frac{-V_{diff}}{2} e^{\frac{-2t}{\tau}} - \frac{V_{diff} V_i}{R_{eq}} e^{\frac{-t}{\tau}})dt \quad (5.3)$$

The difference in capacitor energy provides the energy transferred between two ad-

Table 5.2: Efficiency

| **Cell** | **Initial voltage(V)** | **differential voltage(mV)** | **Energy loss** | **Energy loss (45h)** |
|---|---|---|---|---|
| Cell1 | 3.242 | V1-V2=65 | 0.0083Wh/h | 0.3735Wh |
| Cell2 | 3.307 | V2-V3=119 | 0.0185Wh/h | 0.83Wh |
| Cell3 | 3.419 | V3-V4=248 | 0.06Wh/h | 2.96Wh |
| Cell4 | 3.170 | | | |

jacent cells. So,difference between integral of equation.(5.2) and equation.5.3 will provide the energy loss, then the efficiency. Where $V_{diff}$ is the differential voltage between cells, $\tau$ is the time constant where C is $22\mu F$ and R is the sum of ESR,$R_{on}$ and internal cell resistance at 50kHz.

# Chapter 6

# Conclusions and future work

## 6.1 Conclusions

The rapid developed in electric vehicles and systems working isolated from the grid, make energy storage systems a key element, being batteries one of the most popular. Although, battery systems are widely studied, the vast majority of researches are focused on electrochemical static models and low frequency internal impedance analysis. The most important part of this work was to study the evolution of the internal impedance cell at high frequency. This is a key from either the converter controllers or filter design point of view. To get knowledge of the internal battery impedance when a power converter is switching at a give frequency, provides information to the converter designer in order to avoid resonance with other elements of the system.

In this work was demonstrated, how the internal impedance changes with the frequency. Using the EIS method, differences in cell impedance behaviour have been compared when the battery is resting or when it is working.

The other part of this master thesis is related to cell balancing. Firstly, a review of balancing technology methods have been done. Based on this review, the decision of a cell balancing design was made according to the project needs. Afterwards, a prototype have been simulated and implemented in the lab. The device was designed

to balance four cells, but thinking about the possibility to scale the prototype to balance 255 cells of a module.

## 6.2 Future work

This master thesis is part of a global project called Advanced plug-and-play grid energy generation system and A0 Renewable (OG+). It consists in a distributed generation where the energy storage system is a battery. The battery consists in 15 modules of 255 LiFePO4 cells. The power converter between the battery and the grid must handle 100Kw of power and it is switching at 15kHz. In this master thesis, a scaled power converter like in the real project have been developed. This allows to analysed one cell internal impedance behaviour at the switching frequency. The aim of future researches are to study if this results can be extrapolated to a module of 15x15 matrix cell. Then the work could developed, a dynamic behaviour of the whole battery. Other future work could develop the same experiments, for different chemistry cells and see the difference, or testing the same LiFePO4 chemistry with more cycles of life and compare the results.

Moving on to the cell balancing prototype, the future work could be focused on the efficiency calculation and cost reduction. In addition to this cell balancing at cell level, an active balancing method should be in charge of balancing modules, making a dual balancing scheme.

# Bibliography


[1] T. Stuart, F. Fang, X. Wang, C. Ashtiani, and A. Pesaran, "A modular battery management system for hevs," tech. rep., SAE Technical Paper, 2002.

[2] J.-W. Shin, G.-S. Seo, C.-Y. Chun, and B.-H. Cho, "Selective flyback balancing circuit with improved balancing speed for series connected lithium-ion batteries," in *Power Electronics Conference (IPEC), 2010 International*, pp. 1180–1184, IEEE, 2010.

[3] D. A. González, *High power Li-ION battery performance: A mechanistic analysis of aging*. PhD thesis, University of Oviedo, 2015.

[4] H. Rahimi-Eichi, U. Ojha, F. Baronti, and M.-Y. Chow, "Battery management system: An overview of its application in the smart grid and electric vehicles," *IEEE Industrial Electronics Magazine*, vol. 7, no. 2, pp. 4–16, 2013.

[5] D. Linden, "Handbook of batteries," in *Fuel and Energy Abstracts*, vol. 4, p. 265, 1995.

[6] M. Barak, *Electrochemical power sources: primary and secondary batteries*. No. 1, IET, 1980.

[7] "www.batteryuniversity.com,"

[8] M. Einhorn, V. F. Conte, C. Kral, J. Fleig, and R. Permann, "Parameterization of an electrical battery model for dynamic system simulation in electric vehicles," in *Vehicle Power and Propulsion Conference (VPPC), 2010 IEEE*, pp. 1–7, IEEE, 2010.

[9] M. Sayegh, C. Forgez, T.-H. Tran, and G. Cherouvrier, "Lifepo 4/graphite battery modelling for an aeronautical application," in *Industrial Electronics (ISIE), 2015 IEEE 24th International Symposium on*, pp. 1278–1283, IEEE, 2015.

[10] S. Buller, M. Thele, E. Karden, and R. W. De Doncker, "Impedance-based nonlinear dynamic battery modeling for automotive applications," *Journal of Power Sources*, vol. 113, no. 2, pp. 422–430, 2003.

[11] E. Karden, S. Buller, and R. W. De Doncker, "A method for measurement and interpretation of impedance spectra for industrial batteries," *Journal of Power sources*, vol. 85, no. 1, pp. 72–78, 2000.

[12] L. Gagneur, A. Driemeyer-Franco, C. Forgez, and G. Friedrich, "Modeling of the diffusion phenomenon in a lithium-ion cell using frequency or time domain identification," *Microelectronics Reliability*, vol. 53, no. 6, pp. 784–796, 2013.

[13] E. Kuhn, C. Forgez, P. Lagonotte, and G. Friedrich, "Modelling ni-mh battery using cauer and foster structures," *Journal of power sources*, vol. 158, no. 2, pp. 1490–1497, 2006.

[14] G. Instruments, "Basics of electrochemical impedance spectroscopy," *G. Instruments, Complex impedance in Corrosion*, pp. 1–30, 2007.

[15] J. Cao, N. Schofield, and A. Emadi, "Battery balancing methods: A comprehensive review," in *Vehicle Power and Propulsion Conference, 2008. VPPC'08. IEEE*, pp. 1–6, IEEE, 2008.

[16] S. W. Moore and P. J. Schneider, "A review of cell equalization methods for lithium ion and lithium polymer battery systems," tech. rep., SAE Technical Paper, 2001.

[17] M. Daowd, N. Omar, P. Van Den Bossche, and J. Van Mierlo, "Passive and active battery balancing comparison based on matlab simulation," in *Vehicle Power and Propulsion Conference (VPPC), 2011 IEEE*, pp. 1–7, IEEE, 2011.

[18] A. Manenti, A. Abba, A. Merati, S. M. Savaresi, and A. Geraci, "A new bms architecture based on cell redundancy," *IEEE Transactions on Industrial Electronics*, vol. 58, no. 9, pp. 4314–4322, 2011.

[19] K. B. Hatzell, A. Sharma, and H. K. Fathy, "A survey of long-term health modeling, estimation, and control of lithium-ion batteries: Challenges and opportunities," in *American Control Conference (ACC), 2012*, pp. 584–591, IEEE, 2012.

[20] H. Rahimi-Eichi and M.-Y. Chow, "Adaptive parameter identification and state-of-charge estimation of lithium-ion batteries," in *IECON 2012-38th Annual Conference on IEEE Industrial Electronics Society*, pp. 4012–4017, IEEE, 2012.

[21] T. Huria, M. Ceraolo, J. Gazzarri, and R. Jackey, "Simplified extended kalman filter observer for soc estimation of commercial power-oriented lfp lithium battery cells," tech. rep., SAE Technical Paper, 2013.

[22] G. P. Rodriguez, *Advanced closed loop algorithm for state of charge and state of health estimation in Li-ion batteries at wide operating conditions.* PhD thesis, University of Mondragon, 2016.

[23] "www.liionbms.com,"

[24] C. Pascual and P. T. Krein, "Switched capacitor system for automatic series battery equalization," in *Applied Power Electronics Conference and Exposition, 1997. APEC'97 Conference Proceedings 1997., Twelfth Annual*, vol. 2, pp. 848–854, IEEE, 1997.

[25] M. Green, "Design calculation fro buck-boost converters," *Application report, Texas Instrument*, pp. 1–12, 2012.

[26] C. W. T. McLyman, *Transformer and inductor design handbook*. CRC press, 2016.

[27] T. A. Lipo, *Vector control and dynamics of AC drives*, vol. 41. Oxford university press, 1996.

[28] G. F. Franklin, J. D. Powell, A. Emami-Naeini, and J. D. Powell, *Feedback control of dynamic systems*, vol. 3. Addison-Wesley Reading, MA, 1994.

[29] T. instrument, "Tms320x2833x, 2823x enhanced pulse width modulator (epwm) module," *Application report, Texas Instrument*, p. 24, 2008-2009.

[30] T. Hansen and C.-J. Wang, "Support vector based battery state of charge estimator," *Journal of Power Sources*, vol. 141, no. 2, pp. 351–358, 2005.

[31] J. Remmlinger, M. Buchholz, M. Meiler, P. Bernreuter, and K. Dietmayer, "State-of-health monitoring of lithium-ion batteries in electric vehicles by on-board internal resistance estimation," *Journal of Power Sources*, vol. 196, no. 12, pp. 5357–5363, 2011.

[32] M. Dubarry, V. Svoboda, R. Hwu, and B. Y. Liaw, "Incremental capacity analysis and close-to-equilibrium ocv measurements to quantify capacity fade in commercial rechargeable lithium batteries," *Electrochemical and solid-state letters*, vol. 9, no. 10, pp. A454–A457, 2006.

[33] S. P. Bayon.L, Grau JM, *Metodos matemáticos de la ingeniería*, vol. 3. University of Oviedo, 1994.

[34] M. Daowd, M. Antoine, N. Omar, P. Van den Bossche, and J. Van Mierlo, "Single switched capacitor battery balancing system enhancements," *Energies*, vol. 6, no. 4, pp. 2149–2174, 2013.